Isomeric states observed in heavy neutron-rich nuclei populated in the fragmentation of a ^{208}Pb beam

S. J. Steer,[1] Zs. Podolyák,[1,*] S. Pietri,[1] M. Górska,[2] H. Grawe,[2] K. H. Maier,[3,4] P. H. Regan,[1] D. Rudolph,[5]
A. B. Garnsworthy,[1,6] R. Hoischen,[5] J. Gerl,[2] H. J. Wollersheim,[2] F. Becker,[2] P. Bednarczyk,[2,4] L. Cáceres,[2,7] P. Doornenbal,[2,8]
H. Geissel,[2] J. Grębosz,[2,4] A. Kelic,[2] I. Kojouharov,[2] N. Kurz,[2] F. Montes,[2] W. Prokopwicz,[2] T. Saito,[2] H. Schaffner,[2]
S. Tashenov,[2] A. Heinz,[6] M. Pfützner,[9] T. Kurtukian-Nieto,[10] G. Benzoni,[11] A. Jungclaus,[12] D. L. Balabanski,[13,14] M. Bowry,[1]
C. Brandau,[1] A. Brown,[1,15] A. M. Bruce,[16] W. N. Catford,[1] I. J. Cullen,[1] Zs. Dombrádi,[17] M. E. Estevez,[18] W. Gelletly,[1]
G. Ilie,[8,19] J. Jolie,[8] G. A. Jones,[1] M. Kmiecik,[4] F. G. Kondev,[20] R. Krücken,[21] S. Lalkovski,[16,22] Z. Liu,[1] A. Maj,[4] S. Myalski,[4]
S. Schwertel,[21] T. Shizuma,[1,23] P. M. Walker,[1] E. Werner-Malento,[2] and O. Wieland[1]

[1]*Department of Physics, University of Surrey, Guildford, GU2 7XH, United Kingdom*
[2]*GSI, Planckstrasse 1, D-64291, Darmstadt, Germany*
[3]*University of West of Scotland, Paisley, PA1 2BE, United Kingdom*
[4]*The Institute of Nuclear Physics, PL-31-342, Kraków, Poland*
[5]*Department of Physics, Lund University, S-22100, Lund Sweden*
[6]*WNSL, Yale University, 272 Whitney Avenue, New Haven, Connecticut, 06520, USA*
[7]*Departmento de Fisica Teórica, Universidad Autonoma de Madrid, Madrid, Spain*
[8]*IKP, Universität zu Köln, D-50937, Köln, Germany*
[9]*Faculty of Physics, University of Warsaw, Hoża 69, PL-00-681, Poland*
[10]*Universidad de Santiago de Compostela, Santiago de Campostela, Spain*
[11]*INFN sezione di Milano, I-20133, Milano, Italy*
[12]*Instituto de Estructura de la Materia, CSIC, E-28006 Madrid, Spain*
[13]*INRNE, Bulgarian Academy of Sciences, BG-1784 Sofia, Bulgaria*
[14]*Dipartimento di Fisica, Università di Camerino and INFN-Perugia, I-62032, Italy*
[15]*NSCL, Michigan State University, East Lansing, Michigan 48824-1321, USA*
[16]*School of Engineering, University of Brighton, Brighton, BN2 4GJ, United Kingdom*
[17]*Institute for Nuclear Research, H-4001, Debrecen, Hungary*
[18]*Instituto de Fisica Corpuscular, Valencia, Spain*
[19]*National Institute of Physics and Nuclear Engineering, Bucharest, Romania*
[20]*Nuclear Engineering Division, Argonne National Laboratory, Argonne, Illinois 60439, USA*
[21]*Physik Department E12, Technische Universität München, Garching, Germany*
[22]*Faculty of Physics, University of Sofia "St. Kliment Ohridski," Sofia, Bulgaria*
[23]*Japan Atomic Energy Research Institute, Kyoto, 619-0215, Japan*

Heavy neutron-rich nuclei were populated via the fragmentation of a $E/A = 1$ GeV $^{208}_{82}$Pb beam. Secondary fragments were separated and identified and subsequently implanted in a passive stopper. By the detection of delayed γ rays, isomeric decays associated with these nuclei have been identified. A total of 49 isomers were detected, with the majority of them observed for the first time. The newly discovered isomers are in $^{204,205}_{80}$Hg, $^{201,202,204,205}_{79}$Au, $^{197,203,204}_{78}$Pt, $^{195,199-203}_{77}$Ir, $^{193,197-199}_{76}$Os, $^{196}_{75}$Re, $^{190,191}_{74}$W, and $^{189}_{73}$Ta. Possible level schemes are constructed and the structure of the nuclei discussed. To aid the interpretation, shell-model as well as BCS calculations were performed.

I. INTRODUCTION

Low-lying yrast excited states of closed shell and near-closed shell nuclei provide excellent opportunities to study specific nuclear orbitals of the nucleus [1]. This is because the dominant contributions to their wave-functions comes from only a few nuclear orbits. In the case of nuclei with a $^{208}_{82}$Pb closed core, there is relatively limited experimental information available on neutron-rich species. For example, prior to the present experiment studies on the $N = 126$

isotones below $Z = 82$ have been limited to measurements of excited states in $^{207}_{81}$Tl [2] and $^{206}_{80}$Hg [3–5] and the ground state of $^{205}_{79}$Au [6].

Moving further from ^{208}Pb, the neutron-rich W-Os-Pt nuclei are characterized by different shapes in their ground states, namely prolate, oblate, triaxial, and near $N = 126$, spherical shapes. The lighter isotopes are prolate deformed. By adding more and more neutrons, the shape becomes oblate [7–9]. The exact place where this change occurs is element dependent. Shape transitional nuclei are difficult to treat theoretically, consequently the properties of nuclei in this region are considered to provide a crucial testing ground for nuclear models.

*z.podolyak@surrey.ac.uk

Projectile fragmentation at intermediate and relativistic energies has proved to be an effective way of populating states in nuclei far from the valley of stability. The highest sensitivity is achieved with decay (both internal isomeric-decay and β-decay) spectroscopy. In this paper, experimental information obtained on a large number of heavy neutron-rich nuclei of the elements Ta→Tl ($Z = 73 \rightarrow 81$) is presented. The experiment, performed in 2006, was part of the RISING stopped-beam campaign [10].

II. EXPERIMENTAL TECHNIQUE

An $E/A = 1$ GeV $^{208}_{80}$Pb^{+67} beam was delivered by the GSI UNILAC and SIS-18 accelerator complex. The beam was fragmented on a Be target of thickness 2.526 g/cm^2. The target was backed by a 0.223 g/cm^2-thick Nb foil, to optimize electron stripping of the outgoing fragments. The nuclei of interest, populated via fragmentation processes, were separated and identified using the fragment separator (FRS) [11]. The FRS was operated in standard achromatic mode. The matter at the midfocal plane of the FRS consisted of a 4.9 g/cm^2 Al degrader, followed by a 0.35 g/cm^2 scintillation detector used for time-of-flight (TOF) and position measurements, and another Nb foil (0.108 g/cm^2 thick) to maximize electron stripping.

At the final focal plane of the FRS, a series of detectors characterized the beam. The nuclei passed through two multi-wire detectors for position measurements; two multi sampling ionization chamber (MUSIC) detectors to measure the rate of energy loss of particles, ΔE ($\propto Z^2$); and three scintillation detectors, for timing, position, and energy measurements. A variable thickness homogeneous Al degrader was used to slow down the beam particles, which were finally implanted into a passive plastic stopper. A schematic view of the experimental setup is shown in Fig. 1. The scintillation detectors placed in front of and behind the catcher allowed the offline suppression of the majority of fragments undergoing secondary reactions in the slowing-down process or those which were not stopped in the catcher.

The catcher was surrounded by the high-efficiency, high-granularity stopped RISING γ-ray spectrometer [10,12], which has a full-energy peak efficiency of 15% at 662 keV. Time-correlated γ decays from individually identified ions

have been measured, allowing unambiguous identification of isomeric decays.

Multiple electronic branches recorded the time of emission of γ rays. XIA digital γ finder (DGF) modules recorded γ-ray information with 25-ns resolution for up to 380 μs following implantation. Two other timing circuits were also used. These are termed the short-range (SR) timing circuit, operating with 0.293-ns resolution for an effective 850 ns and long-range (LR) circuit, operating with 0.7629-ns resolution for 100 μs following implantation. The use of the short-range timing is advantageous in the case of short-lived isomeric decays ($<$300 ns).

From synthesis of the fragmentation products at the target to implantation in the stopper approximately 300 ns elapsed. During this in-flight period, electron conversion branches of excited states were suppressed by the high degree of ionization of the nuclei. This had the effect of extending the half-life of the excited states for the in-flight period. Therefore, the experiment was sensitive to the decay of metastable states that are transmitted through the FRS and then decayed in the 380 μs following implantation. In general, this experimental setup can measure isomers with half-lives in the range 10 ns–1 ms.

During the experiment, nine different magnetic rigidity settings of the FRS were used. The results from six of these, dealing with heavy neutron-rich nuclei, are presented in this paper. In these cases, the magnetic rigidities were set to transmit fully stripped ions of ^{206}Hg, ^{203}Ir, ^{202}Os, ^{199}Os, ^{192}W, and ^{185}Lu. An average of 20 h of beam time was dedicated to each setting, with a primary beam intensity of $\sim 10^9$ ions/22 s spill. Details summarizing which species and how many nuclei were implanted during the experiment are information given in Ref. [13], with a more detailed breakdown of this information is given in the PhD thesis [14]. The other three settings, centered at $^{188}_{82}$Pb, $^{186}_{82}$Pb, and $^{147}_{64}$Gd [15,16], aimed at the study of the fragmentation reaction mechanism, and in particular the angular momentum population probability [17].

As a first step in the identification of the nuclei, a charge state selection had to be performed. Charge state calculations with the GLOBAL code [18] show that when exiting the Be/Nb target approximately 94% of the fragmentation products of interest were fully ionized (i.e., $q = Z$, also referred to as "fully stripped") and that the remaining 6% had one electron bound to the nucleus ($q = Z - 1$, referred to as being in a "H-like" charge state). Following energy losses at the midfocal
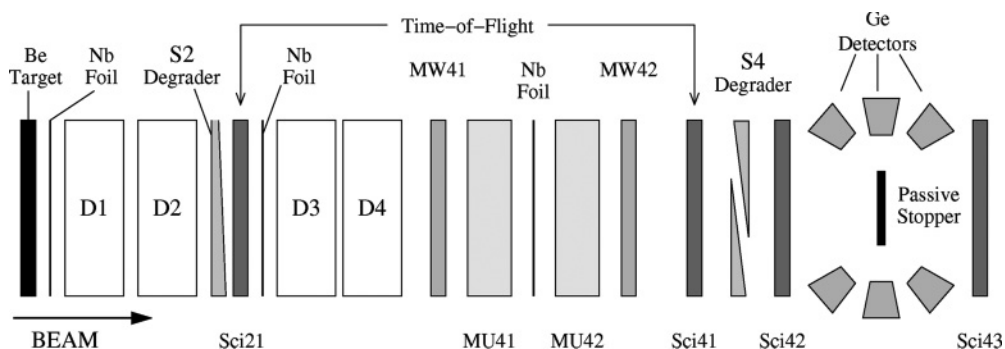

FIG. 1. Schematic of the fragment separator including the used detectors. For details see the text.
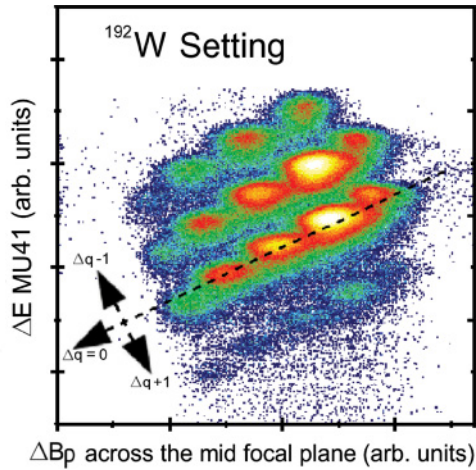
FIG. 2. (Color online) Charge state selection for the ^{192}W setting. The change in the magnetic rigidity at the mid-focal plane, $\Delta B\rho$, is plotted against ΔE ($\propto Z^2$) at the final focal plane measured by the MUSIC detectors. Changes in charge state are identified by the diagonally correlated data.

plane, 77% of the beam was fully stripped of electrons, 22% was in a H-like state, and 1% was in a He-like state ($q = Z - 2$). The matrix energy loss at the final focal plane versus change in magnetic rigidity, $\Delta B\rho$ ($\propto q^2$), at the intermediate focal plane can be used for charge state selection (see Fig. 2). This distinguishes nuclei that do not change charge state in the middle of the FRS (approximately all $\Delta q = 0$ correspond to $q = Z$ for the entire FRS flight time) from those which pick up one or two electrons ($\Delta q = -1$ and $\Delta q = -2$) or lose one electron ($\Delta q = +1$).

The identification plot corresponding to the $^{192}_{74}$W setting is shown in Fig. 3. The analogous pictures for the $^{203}_{77}$Ir and $^{199}_{76}$Os settings can be found in Refs. [19,20], respectively. All identification plots are available in Ref. [14]. Each
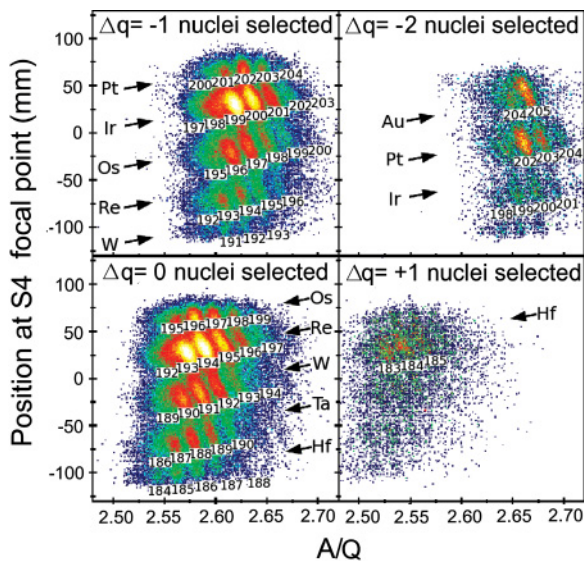

FIG. 3. (Color online) Identification plot for the FRS setting centered on $^{192}_{74}$W. The four figures correspond to different charge state combinations through the fragment separator.
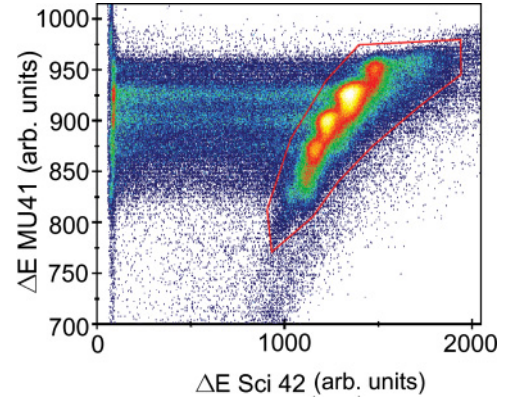

FIG. 4. (Color online) Rate of energy loss of identified beam nuclei before (ΔE MUSIC41) and after (ΔE Sci42) the homogeneous degrader at the final focal plane. The closed line encompasses those nuclei that did not react during the slowing down process.

identification plot has been confirmed by the observation of γ-ray transitions following the decay of previously reported isomers.

Following their identification, the nuclei were slowed down in the homogeneous Al degrader, before being implanted in a passive stopper. In the degrader, the ions were slowed down from an energy of $E/A \sim 400$ MeV to $E/A < 100$ MeV. In the slowing-down process, a number of the nuclei of interest were lost due to reactions in the degrader. A comparison of a ΔE measurement by a MUSIC chamber located upstream from the degrader and one made by the scintillation detector placed immediately following the degrader (Sci42) identifies nuclei that react inside it (see Fig. 4). The latter are removed from further analysis. It was found that $\approx 18\%$ of the nuclei react at this stage.

In the $^{206}_{80}$Hg, $^{203}_{77}$Ir, and $^{202}_{76}$Os settings, the selected beam nuclei were implanted in a 7-mm-thick perspex stopper. For the other three settings, a 9-mm-thick perspex stopper was used. One final scintillation detector (Sci43), placed after the stopper, acted as a veto on events where particles were detected after the stopper, this accounted for $\approx 0.2\%$ of the identified nuclei.

As each nucleus decelerates and comes to a halt in the stopper, bremsstrahlung is emitted, causing the so-called "prompt flash" [21,22]. The prompt flash is measured to have a FWHM ~ 20 ns when using the SR devices at γ-ray energies, $E_\gamma > 500$ keV; this width includes the uncertainty associated with synchronizing the independent time circuits of the 105 Ge crystals. Isomers with half-lives comparable to this width are subject to a large background contribution.

III. RESULTS

The analysis of the data collected in this experiment has identified 49 isomers in 39 nuclear species between Ta ($Z = 73$) and Tl ($Z = 81$). The nuclei with isomeric states are indicated in Fig. 5 and the experimental observables are summarized in Table I. The experimental observables include the intensity of the γ rays, the isomeric lifetime, and the
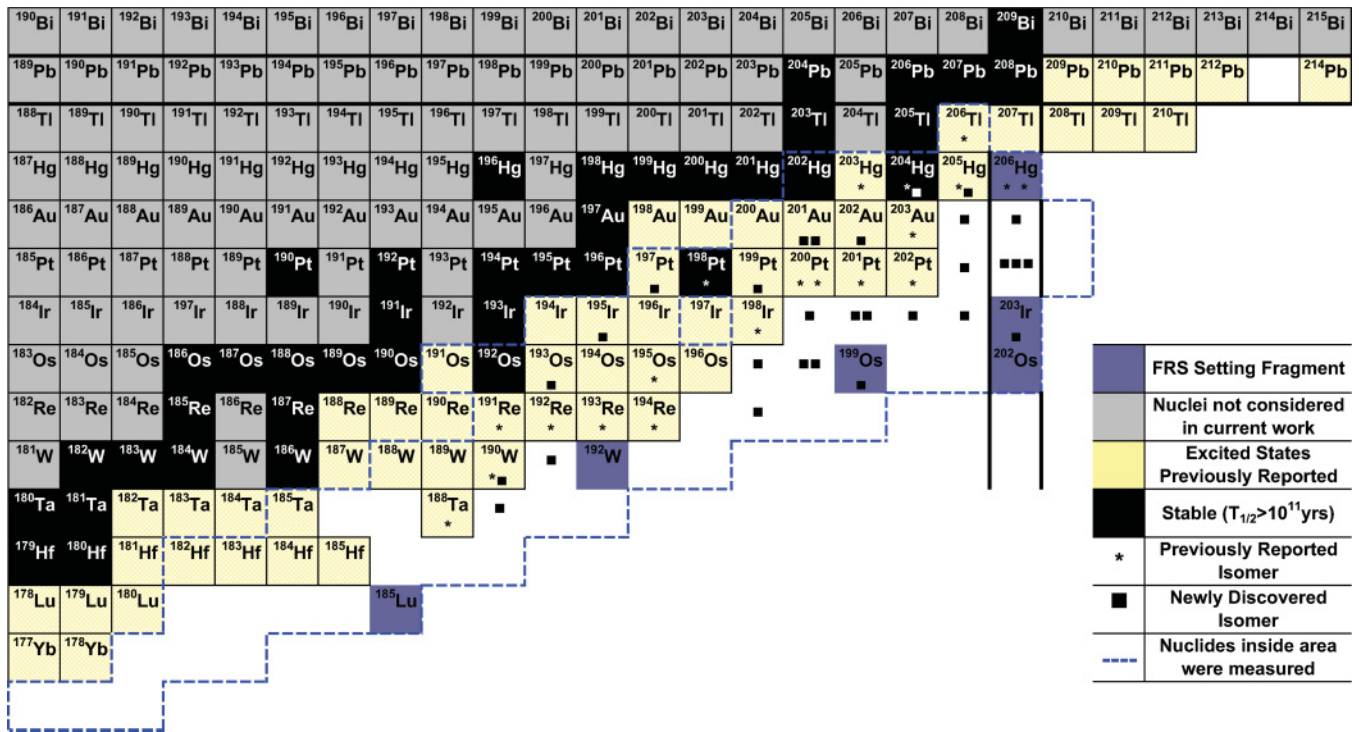
FIG. 5. (Color online) Section of the nuclide chart indicating the nuclei studied in the present experiment. The figure shows the nuclei with observed isomers as well as the nuclei with knowledge on excited states prior to the present experiment.

isomeric ratio. Of the observed isomers, 20 have been already reported prior to performing the described experiment and 29 were observed for the first time.

An isomeric ratio is defined as the number of times a nuclide is populated in an excited state that decays through a given isomer, divided by the total number of times that the nuclide has been populated. A detailed explanation of how this is determined is given in Ref. [23]. Where more than one isomer has been observed in a nucleus, the isomeric ratio of the lower-lying isomer is *inclusive* of any feeding from the higher-lying isomer. If the same nucleus was transmitted in different settings and in different charge states, the isomeric ratios were determined for each charge-state combination separately. The final values are given in Table I. Isomeric states often decay via low-energy highly converted unobserved transitions. Without knowing the energy of the decaying transition, one cannot calculate how many of them decay while flying through the fragment separator. Therefore, only a lower isomeric ratio limit could be determined in these cases, assuming no decays (infinite conversion electron coefficient) during flight through the FRS.

A. Theoretical calculations

We performed shell-model calculations on the nuclei in the vicinity of ^{208}Pb. The OXBASH code [24] was employed. The model space considered consisted of the proton orbitals $3s_{1/2}$, $2d_{3/2}$, $1h_{11/2}$, $2d_{5/2}$, and $1g_{7/2}$ below the $Z = 82$ closed shell and the neutron orbitals $3p_{1/2}$, $2f_{5/2}$, $3p_{3/2}$, $1i_{13/2}$, $2f_{7/2}$, and $1h_{9/2}$ below the closed $N = 126$ shell. Except

for ^{202}Au, where the $\pi g_{7/2}$ and $\nu h_{9/2}$ orbitals were kept filled, no further truncation was applied. Therefore, no core excitations across the ^{208}Pb double-shell closure are allowed. The single proton-hole and neutron-particle energies are taken from the experimental spectra of ^{207}Tl and ^{207}Pb, respectively. The two-body interaction matrix elements (TBMEs) are from Ref. [25]. They are based on the Kuo-Herling interaction [26] including core polarization, with decisive elements adjusted to the experimental data available at the time. We shall refer to this as the standard parametrization.

In addition to the aforedescribed standard parametrization, a modified parametrization was also used. These modifications were introduced to get better agreement between theory and experiment for the new ^{204}Pt and updated ^{206}Hg data [5]. As explained in Ref. [19], the Rydström interaction [25] was modified in three points: (i) the $(d_{3/2} h_{11/2})_{7^-}$ TBME was increased by +135 keV as needed for ^{206}Hg; (ii) the $(s_{1/2} d_{5/2})$ monopole was increased by +230 keV, which accounts for the 4^+ level energy in ^{204}Pt and the increased blocking of the $h_{11/2} \otimes 3^-$ coupling lowering the effective $d_{5/2}$ single hole energy; (iii) following a systematic search of the influence of nondiagonal TBME on the $E2$ strength evolution from ^{206}Hg to ^{204}Pt, the $(s_{1/2} h_{11/2}; d_{3/2} h_{11/2})_{6^-}$ TBME was changed to +160 keV, close to the value for the corresponding 5^- TBME.

Here we examine whether these modifications needed by ^{204}Pt and ^{206}Hg improve the predictive power of the calculations for other nuclei in the region. This is especially important, since such shell-model calculations are used to predict the properties of the $N = 126$ r-process path nuclei [27].

TABLE I. Summary of the observed isomeric states. Half-lives and isomeric ratios, as well as γ-ray energies and relative intensities are given. For details see the text.

Nucleus, I^{π}, $T_{1/2}$, IR (%) E_{γ} (keV)	I_{γ}
^{206}Tl, $I^{\pi} = (5)^{+}$ [30], $T_{1/2} = 71(4)$ ns, IR $= 14.2^{+21}_{-32}$	
265.4	89(6)
452.9	90(6)
685.8	100(7)
^{206}Hg, $I^{\pi} = (10^{+})$ [30], $T_{1/2} = 112(4)$ ns, IR $= 2.2^{+7}_{-8}$	
100.9	3(3)
363.4	21(1)
1156.3	28(1)
1257.2	8(1)
^{206}Hg, $I^{\pi} = 5^{-}$ [30], $T_{1/2} = 2.09(2)$ μs, IR $= 21.9^{+12}_{-29}$	
1033.7	100(2)
1068.0	99(2)
^{205}Hg, $I^{\pi} = (23/2^{-})$, $T_{1/2} = 5.89(18)$ μs, IR $= 3.3^{+2}_{-4}$	
227.6	8(1)
722.6	11(1)
810.0	100(3)
950.2	87(3)
^{205}Hg, $I^{\pi} = 13/2^{+}$, $T_{1/2} = 1.09(4)$ ms [36], IR $= 20.5^{+25}_{-40}$	
378.9	37(2)
967.0	10(2)
1014.7	33(2)
^{204}Hg, $I^{\pi} = (14^{+})$, $T_{1/2} = 20(2)$ ns, IR < 10	
422.7	35(7)
597.2	100(14)
964.8	61(14)
1013.9	30(15)
^{204}Hg, $I^{\pi} = 7^{-}$ [38], $T_{1/2} = 6.7(5)$ ns [38]	
436.6	59(10)
691.8	36(9)
1062.7	36(10)
^{203}Hg, $I^{\pi} = (13/2^{+})$ [39], $T_{1/2} = 21.9(10)$ μs, IR $= 11.8^{+11}_{-20}$	
341.0	57(2)
591.1	100(3)
^{205}Au, $I^{\pi} = (19/2^{+})$, $T_{1/2} = 163(5)$ ns, IR $= 6.5^{+10}_{-15}$	
34.2	–
243.4	4(2)
736.9	39(2)
928.3	23(2)
946.1	94(4)
962.5	100(5)
962.5	11(4)
980.2	24(2)
1171.5	32(2)
^{204}Au, $I^{\pi} = (16^{+})$, $T_{1/2} = 2.1(3)$ μs, IR $= 0.6(2)$	
839.0	100(15)
976.6	93(15)
^{203}Au, $I^{\pi} = 11/2^{-}$, $T_{1/2} = 140(44)$ μs, IR $= 2.5^{+8}_{-10}$	
562.8	100(6)
^{202}Au, $I^{\pi} =$ unknown, $T_{1/2} = 13.1(5)$ ns	
137.8	21(21)
414.2	100(5)

TABLE I. (*Continued*)

Nucleus, I^{π}, $T_{1/2}$, IR (%) E_{γ} (keV)	I_{γ}
^{201}Au, $I^{\pi} = 11/2^{-}$, $T_{1/2} = 340^{+900}_{-290}\mu$s, IR $= 13^{+36}_{-11}$	
553	100(51)
^{201}Au, $I^{\pi} =$ unknown, $T_{1/2} = 5.6(24)\mu$s, IR $= 5(3)$	
378.2	58(17)
638.0	100(34)
^{204}Pt, $I^{\pi} = (10^{+})$, $T_{1/2} = 146(14)$ ns, IR $= 9.2^{+25}_{-32}$	
96.1	2(2)
1060.8	20.7(11)
1157.5	3.7(5)
^{204}Pt, $I^{\pi} = (7^{-})$, $T_{1/2} = 55(3)$ μs, IR $= 27^{+7}_{-9}$	
<78.4	–
^{204}Pt, $I^{\pi} = (5^{-})$, $T_{1/2} = 5.5(7)$ μs, IR $= 40^{+17}_{-20}$	
872.4	100(2)
1122.7	97(2)
^{203}Pt, $I^{\pi} = (33/2^{+})$, $T_{1/2} = 641(55)$ ns, IR $= 1.3(2)$	
1104.0	100(8)
^{202}Pt, $I^{\pi} = 7^{-}$ [67], $T_{1/2} = 141(7)$ μs, IR $= 12^{+1}_{-2}$	
534.3	95(2)
534.3	95(2)
718.8	100(3)
^{201}Pt, $I^{\pi} = (25/2^{-}, 27/2^{-})$, $T_{1/2} = 18.4(13)$ ns, IR $\geqslant 4(2)$	
353.6	76(6)
373.9	80(5)
726.9	100(6)
^{200}Pt, $I^{\pi} = (12^{+})$ [68], $T_{1/2} = 13.9(10)$ ns, IR $\geqslant 2(1)$	
318.4	16(2)
542.5	17(2)
708.6	22(3)
^{200}Pt, $I^{\pi} = 7^{-}$ [68], $T_{1/2} = 17.0(5)$ ns, IR $\geqslant 7(4)$	
298.9	8(2)
397.5	8(2)
401.0	8(2)
463.6	72(3)
470.1	87(3)
633.0	100(4)
^{199}Pt, $I^{\pi} = (25/2^{-}, 27/2^{-})$, $T_{1/2} = 18.6(34)$ ns, IR $\geqslant 5(3)$	
318.9	84(19)
419.6	86(15)
597.4	100(15)
^{198}Pt, $I^{\pi} = 7^{-}$, $T_{1/2} = 3.4(2)$ ns [47]	
382.0	54(16)
407.2	100(29)
577.8	65(25)
^{197}Pt, $I^{\pi} = (25/2^{-}, 27/2^{-})$, $T_{1/2} = 10.2(13)$ ns, IR $\geqslant 5(2)$	
374.5	100(12)
432.2	72(14)
546.9	66(12)
^{203}Ir, $I^{\pi} = (23/2^{+})$, $T_{1/2} = 798(350)$ ns, IR $= 5^{+3}_{-4}$	
207.0	18(8)
841.3	73(21)
894.7	100(25)
^{202}Ir, $I^{\pi} =$ unknown, $T_{1/2} = 3.4(6)$ μs, IR $= 0.7^{+2}_{-3}$	
311.5	41(13)

TABLE I. (*Continued*)

Nucleus, I^π, $T_{1/2}$, IR (%) E_γ (keV)	I_γ
655.9	54(17)
737.2	100(29)
889.2	51(17)
967.6	44(15)
^{201}Ir, I^π = unknown, $T_{1/2}$ = 10.5(17) ns, IR $\geqslant$ 3(2)	
439.6	39(9)
452.0	51(9)
680.9	100(13)
^{200}Ir, I^π = unknown, $T_{1/2}$ = 17.1(12) ns, IR = 22(12)	
120.0	30(2)
^{200}Ir, I^π = unknown, $T_{1/2}$ = 28.5(15) ns, IR = 3.5(14)	
126.6	100(3)
^{199}Ir, I^π = unknown, $T_{1/2}$ = 8.9(5) ns,	
448.5	100(7)
500.2	67(5)
500.2	14(1)
547.2	82(7)
596.6	38(6)
^{198}Ir, I^π = unknown, $T_{1/2}$ = 73(11) ns, IR = 5(4)	
116.4	100(17)
^{195}Ir, I^π = unknown, $T_{1/2}$ = 4.4(6) μs, IR = 1.1^{+2}_{-3}	
268.4	76(19)
404.4	90(30)
476.7	61(28)
537.8	96(29)
566.7	100(30)
^{199}Os, I^π = unknown, $T_{1/2}$ = 25.2(20) ns, IR $\geqslant$ 1.4(7)	
379.3	57(18)
401.8	100(19)
424.8	49(13)
736.5	47(25)
970.6	48(28)
^{198}Os, I^π = (12$^+$), $T_{1/2}$ = 18.0(28) ns, IR $\geqslant$ 0.4(2)	
446.8	11(2)
526.9	10(2)
544.0	6(2)
^{198}Os, I^π = (7$^-$), $T_{1/2}$ = 16.1(8) ns IR $\geqslant$ 5(3)	
329.9	27(3)
412.1	16(3)
465.4	100(4)
473.1	13(2)
607.3	80(4)
608.2	80(4)
885.6	19(3)
^{197}Os, I^π = (25/2$^-$, 27/2$^-$), $T_{1/2}$ = 78.2(66) ns, IR = 4(2)	
204.4	62(12)
415.9	92(9)
486.5	100(10)
628.8	96(11)
^{195}Os, I^π = (25/2$^+$, 29/2$^-$), $T_{1/2}$ = 34.0(23) ns, IR $\geqslant$ 2.4(8)	
438.6	100(11)
493.0	73(10)

TABLE I. (*Continued*)

Nucleus, I^π, $T_{1/2}$, IR (%) E_γ (keV)	I_γ
533.1	73(10)
714.0	90(12)
^{193}Os, I^π = unknown, $T_{1/2}$ = 132(29) ns, IR $\geqslant$ 7(4)	
242.0	100(26)
^{196}Re, I^π = unknown, $T_{1/2}$ = 3.6(6) μs	
x rays	–
^{194}Re, I^π = unknown, $T_{1/2}$ = 45(18) μs, IR = 5(3)	
86.3	100(25)
^{193}Re, I^π = (9/2$^-$), $T_{1/2}$ = 65(9) μs, IR = 16^{+4}_{-5}	
145.2	100(11)
^{192}Re, I^π = unknown, $T_{1/2}$ = 85(10) μs, IR = 3(1)	
159.3	100(9)
^{191}Re, I^π = unknown, $T_{1/2}$ = 77(33) μs	
134.5	42(11)
139.9	40(11)
158.3	57(13)
224.6	100(19)
418.5	65(18)
443.7	42(15)
^{191}W, I^π = unknown, $T_{1/2}$ = 0.36(2) μs	
67.5	100(25)
167.4	50(10)
^{190}W, I^π = unknown, $T_{1/2}$ = 0.35(4) μs	
x rays	–
^{190}W, I^π = (8$^+$), I^π = (10$^-$) [64], $T_{1/2}$ = 108(9) μs	
206.8	81(10)
358.3	92(10)
484.3	100(11)
694.0	71(10)
^{189}Ta, I^π = unknown, $T_{1/2}$ = 0.58(22) μs	
153.9	100(19)
283.7	73(17)
342.5	47(13)
388.7	80(19)
481.6	97(21)
^{188}Ta, I^π = unknown, $T_{1/2}$ = 3.5(4) μs, IR = 8(2)	
291.9	100(7)

Shell model calculations with both the standard and the modified parametrization have been performed for all cases. As the changes involve only proton orbitals, the energy spectra of both calculations are presented only for the N = 126 nuclei. In $N < 126$ nuclei, the differences in the energy spectra are generally small and only the energy spectra of the modified parametrization are given. Transition rates were calculated using effective operators as listed in Table II. The effective charges and g factors were adjusted to transitions in the one- and two-hole neighbors of ^{208}Pb. The measured transition strengths are compared with both shell model calculations for all nuclei for which such calculations could be performed (see Table II).

TABLE II. Experimental and calculated transition strengths. Both the calculated Rydström [25] shell model (SM)$_{standard}$ and the new TBMEs (SM$_{mod}$) values are given. The following effective operators were used: $e_\pi = 1.5e$ and $e_\nu = 0.85e$ for E2 and E5 transitions, $e_\pi = 2.0e$ and $e_\nu = 2.5e$ for E3 and E4 transitions, $g_s = 0.7g_s^{free}$ for M1 and M2 transitions, and $g_s = 0.35g_s^{free}$ for M4. See the text for details.

Nucleus	Transition	B(EL) (W.u.)		
		exp.	SM$_{standard}$	SM$_{mod}$
^{206}Hg	$B(E3 : 10^+ \rightarrow 7^-)$	0.25(3) [5]	0.17	0.21
^{206}Hg	$B(E2 : 10^+ \rightarrow 8^+)$	0.94(15) [5]	0.87	0.87
^{206}Hg	$B(E3 : 5^- \rightarrow 2^+)$	0.18(2) [5]	1.17	0.90
^{205}Au	$B(E3 : 19/2^+ \rightarrow 13/2^-)$	0.3(1)	0.004	0.02
	or			
	$B(E3 : 19/2^+ \rightarrow 15/2^-)$	0.3(1)	1.0	1.10
^{205}Au	$B(E2 : 19/2^+ \rightarrow 15/2^+)$	1.2(2)	2.99	1.70
^{205}Au	$B(M4 : 11/2^- \rightarrow 3/2^+)$	$\leqslant$1.7(7) [34]	1.92	2.46
^{204}Pt	$B(E3 : 10^+ \rightarrow 7^-)$	0.19(3)	0.21	0.21
^{204}Pt	$B(E2 : 10^+ \rightarrow 8^+)$	0.80(8)	2.64	1.22
^{204}Pt	$B(E2 : 7^- \rightarrow 5^-)$	0.017+ $\rightarrow$0.0034^a	1.21	0.0037
^{204}Pt	$B(E3 : 5^- \rightarrow 2^+)$	0.039(5)	0.713	0.612
^{203}Ir	$B(E2 : 23/2^+ \rightarrow 19/2^+)$	0.020(9)	3.58	0.013
	or			
	$B(E3 : 19/2^+ \rightarrow 15/2^-)$	1.3(6)	0.39	0.44
	or			
	$B(E3 : 19/2^+ \rightarrow 13/2^-)$	1.3(6)	0.144	0.50
^{205}Hg	$B(E3 : 23/2^- \rightarrow 17/2^+)$	0.10(1)	1.80	1.34
^{205}Hg	$B(M2 : 23/2^- \rightarrow 19/2^+)$	8(1)$\times 10^{-5}$	0.008	0.009
^{205}Hg	$B(E3 : 13/2^+ \rightarrow 7/2^-)$	1.14(7) [36]	3.50	3.38
^{205}Hg	$B(M2 : 13/2^+ \rightarrow 9/2^-)$	4.7(3)$\times 10^{-4}$ [36]	0.03	0.03
^{204}Au	$B(M2 : 16^+ \rightarrow 14^-)$	4.7(8)$\times 10^{-4}$	3.5×10^{-4}	21×10^{-4}
	or			
	$B(E3 : 16^+ \rightarrow 14^-)$	0.28(5)	0.80	0.83
^{203}Pt	$B(E3 : 33/2^+ \rightarrow 27/2^-)$	0.38(4)	0.30	0.32
^{203}Hg	$B(M2 : 13/2^+ \rightarrow 9/2^-)$	0.0457(21)	0.05	0.045
^{203}Au	$B(M2 : 11/2^- \rightarrow 7/2^+)$	0.03(2)	0.035	0.034
^{202}Pt	$B(E3 : 7^- \rightarrow 4^+)$	0.268(13)	0.09	0.058

^{a}Assuming a transition energy between $10 \rightarrow 78$ keV.

In the case of deformed nuclei, multi-quasi-particle calculations were performed with a BCS blocking code [28]. The deformation parameters were taken from Ref. [29].

B. N = 126 nuclei

Isomeric decays were observed in four $N = 126$ nuclei: ^{206}Hg, ^{205}Au, ^{204}Pt, and ^{203}Ir. The associated delayed γ-ray spectra are shown in Fig. 6.

Previously, experimental information existed only on the excited states of ^{206}Hg, where two isomeric states were identified. These are an $I^\pi = 5^-$, $T_{1/2} = 2.15(21)$ μs state [3–5,30] and an $I^\pi = (10^+)$, $T_{1/2} = 92(8)$ ns state [5,30], which has 100% feeding to the lower-lying isomer. Our measured half-lives of $T_{1/2} = 2.09(2)$ μs and $T_{1/2} = 112(4)$ ns agree with the previously published values. The determined isomeric ratios, given in Table I, are in fair agreement with the predictions of two nucleon removal reaction theory, as discussed in Ref. [31]. In addition, the dependence of the isomeric ratio of the 5^- state on the transferred longitudinal

momentum was compared with the theoretical calculations [32].

In ^{205}Au, an isomeric state with $T_{1/2} = 163(5)$ ns was observed. In ^{204}Pt three isomeric states with half-lives of 146(14) ns, 55(3) μs, and 5.5(7) μs were identified. The data on these nuclei have already been discussed in detail in Refs. [19,20], respectively.

In the case of $^{203}_{77}$Ir two γ-ray transitions were observed, with energies of 841 and 895 keV. The half-life of the isomer is measured to be $T_{1/2} = 0.8(4)$ μs. There is a candidate for a third γ-ray transition with 207 keV energy.

The shell-model predictions and interpretation of experimental data are presented in Fig. 7. In the case of ^{204}Pt [19], based on similarities with ^{206}Hg as well as shell model predictions, the three isomeric states were interpreted as $I^\pi = (5^-)$, (7^-), and (10^+) with $\pi h_{11/2}^{-1}s_{1/2}^{-1}$, $\pi h_{11/2}^{-1}d_{3/2}^{-1}$, and $\pi h_{11/2}^{-2}$ predominant configurations, respectively.

In ^{205}Au, the yrast structure has been established up to spin-parity $(19/2^+)$ via the observation of the decay of an isomeric state with configuration $\pi(h_{11/2}^{-2})_{10}(s_{1/2}^{-1})$ (for details see Ref. [20]). This isomer feeds into the long-lived $11/2^-$ state
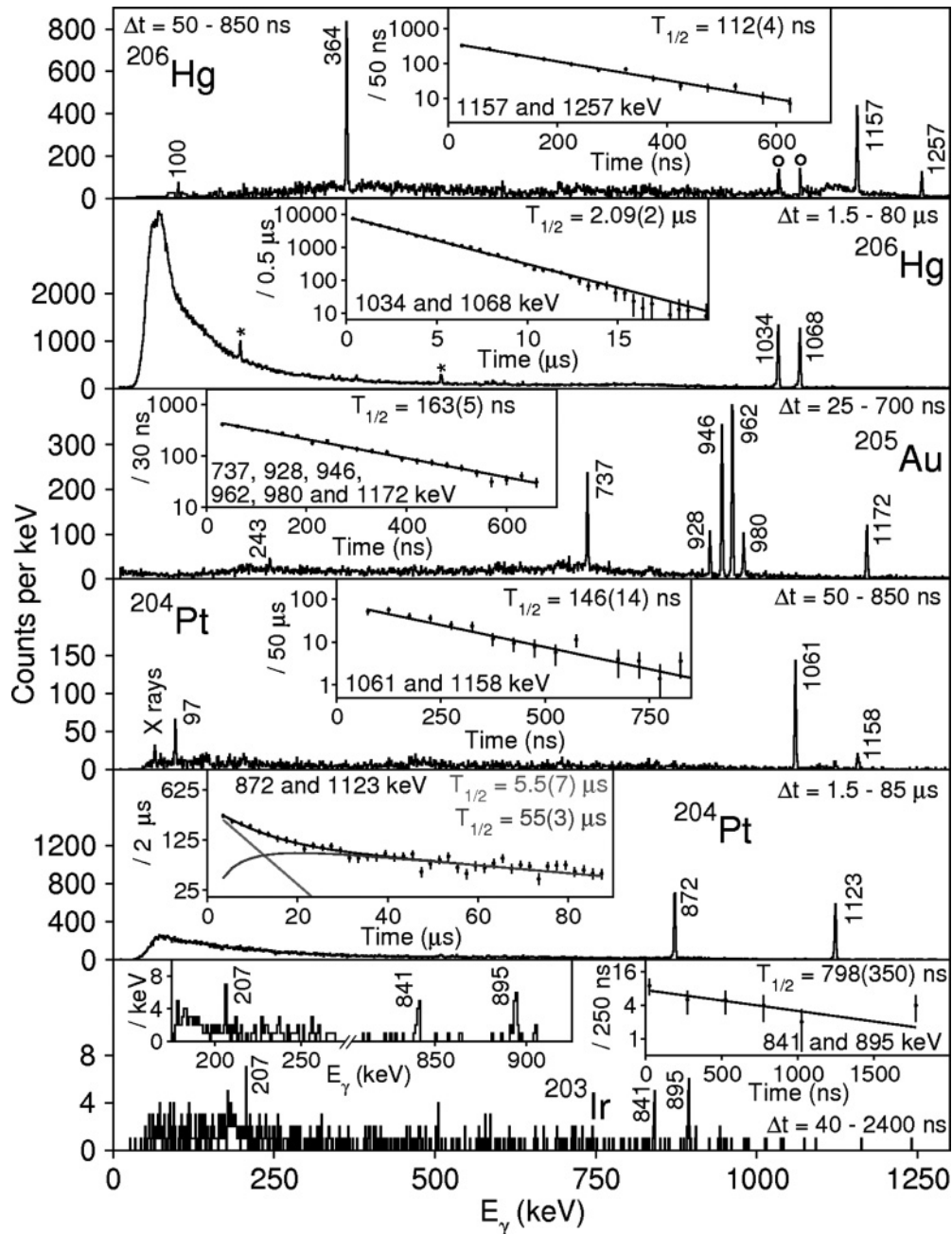
FIG. 6. Delayed γ-ray energy spectra for $N = 126$ nuclei. Background peaks are indicated by $\star$. The peaks indicated by $\circ$ belong to the nucleus of interest, but originate from a different isomeric state than that for which the time limits of the γ spectrum are optimised. Inset spectra are time curves associated with the decay of the observed isomers. The transitions used to measure half-lives are indicated in the time spectra. For ^{203}Ir, the inset presents an expanded γ-ray energy spectrum to highlight the observed energy peaks.

with $\pi h_{11/2}^{-1}$ configuration. This latter state has been identified and its lifetime measured in a later RISING experiment using an active Si stopper [33], by observing the conversion electron associated with the $\pi h_{11/2}^{-1} \rightarrow \pi d_{3/2}^{-1}$ transition [34]. The higher-lying, $19/2^+$, isomer decays into the yrast $15/2^+$ state by a low-energy E2 transition. In addition, it decays by a 963 keV transition into a state that can have spin-parity of either $13/2^-$ or $15/2^-$. The shell-model calculations predict that even if it is $15/2^-$, the transition will have predominantly E3 character

with only a very small, $\sim 10^{-5}$ W.u., M2 admixture. The $15/2^+$ state decays by three high-energy transitions to states with $I^\pi = (13/2^-, 15/2^-)$.

In ^{203}Ir, similarly to ^{205}Au, the observed isomeric state is expected to decay into the $11/2^-$ long-lived level. The isomer is likely to have a spin in the $19/2$–$23/2$ range. There are two possible scenarios. One is that the isomer is similar to that in ^{205}Au, so has $I^\pi = 19/2^+$ and it decays to the $15/2^+$ state by a low energy E2 transition. Alternatively, the isomer

FIG. 7. Experimental and calculated partial level schemes of the $N = 126$ ^{206}Hg [5], ^{204}Pt, ^{205}Au and ^{203}Ir nuclei. Arrow widths denote relative intensities of parallel decay branches. The dominant state configurations are indicated. Theory (a) represents calculations using the Rydström matrix elements, while (b) are with the modified ones, as described in the text.

has $I^\pi = 23/2^+$ and it decays to the $19/2^+$ state, possibly via the 207 keV tentative γ-ray transition. In this case, the $19/2^+$ state is most likely isomeric as well, decaying by a strong E3 into either a $13/2^-$ or $15/2^-$ state. Based on the shell-model calculations, we are inclined toward this second scenario. The existence of two isomeric states would explain the lower intensity of the tentative 207 keV transition. The transition strength was determined assuming the same half-life for both metastable states (Table II).

We compare the standard and the modified shell model calculations with the experimental data, with the energy spectra presented in Fig. 7, and with the reduced transition strengths in Table II. The main differences are: (i) the modified shell model gives a better description of the decay of the long-lived $11/2^-$ isomer in ^{205}Au. According to the calculations, the isomer should decay via an E3 transition into the yrast $5/2^+$ state with a partial half-life of the order of ∼0.1 s. This is contradicted by the experiment as the measured half-life is much longer [34]. The $5/2^+$ state cannot be as low as predicted by the standard shell model, it is likely that it lies above the $11/2^-$ state; (ii) the B(E2 :$19/2^+ \rightarrow 15/2^+$) transition strength in ^{205}Au is described much better by the modified shell model; (iii) in ^{203}Ir the modified shell-model gives a low B(E2) transition strength for the transition depopulating the isomer, in agreement with the experiment. (iv) the modified shell model calculation predicts a much longer half-life (when compared with the standard calculations) for the $11/2^-$ state in ^{203}Ir. However, in this case we do not have experimental information. Based on the above evidence, (i), (ii), and (iii) we conclude that the modifications of the shell-model TBMEs improve the description of the odd-A ^{205}Au and ^{203}Ir nuclei.

C. $N = 125$ nuclei

Isomeric decays were observed in five $N = 125$ nuclei: ^{206}Tl, ^{205}Hg, ^{204}Au, ^{203}Pt, and ^{202}Ir. The corresponding delayed γ-ray spectra are shown in Fig. 8.

Two of the observed isomers and their decay have been reported previously. These are the $I^\pi = (5)^+$, $T_{1/2} = 78(1)$ ns [30,35] isomeric state in ^{206}Tl, and the $I^\pi = 13/2^+$, $T_{1/2} = 1.09(4)$ ms [36] isomer in ^{205}Hg. The lifetime of $T_{1/2} = 71(4)$ ns for ^{206}Tl measured in the present experiment agrees with the published value. We could not determine the half-life of the above mentioned isomeric state in ^{205}Hg since our correlation time, 85 μs in this case, was much shorter than the lifetime.

In ^{205}Hg a previously unreported isomer has also been detected. Transitions with energies of 228, 723, 810, and 950 keV have been observed. The isomer has a lifetime of $T_{1/2} = 5.89(18)$ μs. Time differentiated γ-γ coincidence analysis proves that this newly discovered isomer feeds the previously observed $I^\pi = 13/2^+$ isomer. Within experimental uncertainties the sum of the energies of the 228 and 723 keV transitions is equal to the 950 keV transition, indicating that these are parallel decay pathways, which was confirmed by γ-γ coincidence analysis. All these three transitions are in coincidence with the 810 keV line.

In ^{204}Au excited states have been observed for the first time. Transitions are detected at the energies 839 and 977 keV. The half-life of the isomer is $T_{1/2} = 2.1(3)$ μs. There are other, tentatively identified γ-ray transitions at energies of 97, 277, 427, and 704 keV [14]. We note that recently the β decay of ^{204}Pt was studied and γ rays belonging to ^{204}Au, with energies of 165 and 305 keV, in mutual coincidence, were reported [37].

In ^{203}Pt, one transition has been identified, with an energy of 1104 keV and associated half-life of $T_{1/2} = 641(55)$ ns.

In ^{202}Ir, no experimental observation was available prior to this work. γ rays with energies of 312, 656, 737, 889, and 968 keV and Ir K x rays were detected. A parallel decay branch is likely as the sum of the energy of the 312 and 656 keV transitions is equal to 968 keV, within experimental uncertainties. The half-life of the isomer is determined to be $T_{1/2} = 3.4(6)$ μs.

The experimental and calculated level schemes of the $N = 125$ nuclei are shown in Fig. 9. In ^{205}Hg, the low

energy part is dominated by single-neutron orbitals. The $p_{1/2}$, $f_{5/2}$, $p_{3/2}$, and $i_{13/2}$ neutron holes are associated with the 0, 379, 468, and 1556 keV states. The latter one is isomeric. All the yrast states above 2 MeV must involve at least three unpaired holes. The calculations suggest that the $23/2^-$ state should be isomeric and decaying into the yrast $17/2^+$ and $19/2^+$ states. The $23/2^-$ and $19/2^+$ states have predominant $\pi(s_{1/2}^{-1}h_{11/2}^{-1})5^- \nu i_{13/2}^{-1}$ and $\pi(d_{3/2}^{-1}h_{11/2}^{-1})7^- \nu f_{5/2}^{-1}$ configurations, respectively, while the $17/2^+$ state

has a leading $\pi(s_{1/2}, d_{3/2})^{-2}2^+ \nu i_{13/2}^{-1}$ configuration. Therefore, the parity changing M2 and E3 transitions will be hindered as they proceed via minority components in the wave functions. We associate these decay out transitions with the observed 950 and 723 keV γ rays. Assuming that both transitions are stretched, the deduced transition strengths are B(E3; 950 keV) = 0.10(1) W.u. and B(M2; 723 keV) = 8(1)×10^{-5} W.u. The E3 transition is mediated by the $\pi h_{11/2} \to \pi d_{5/2}$ conversion; i.e., the weak $d_{5/2}$ content in
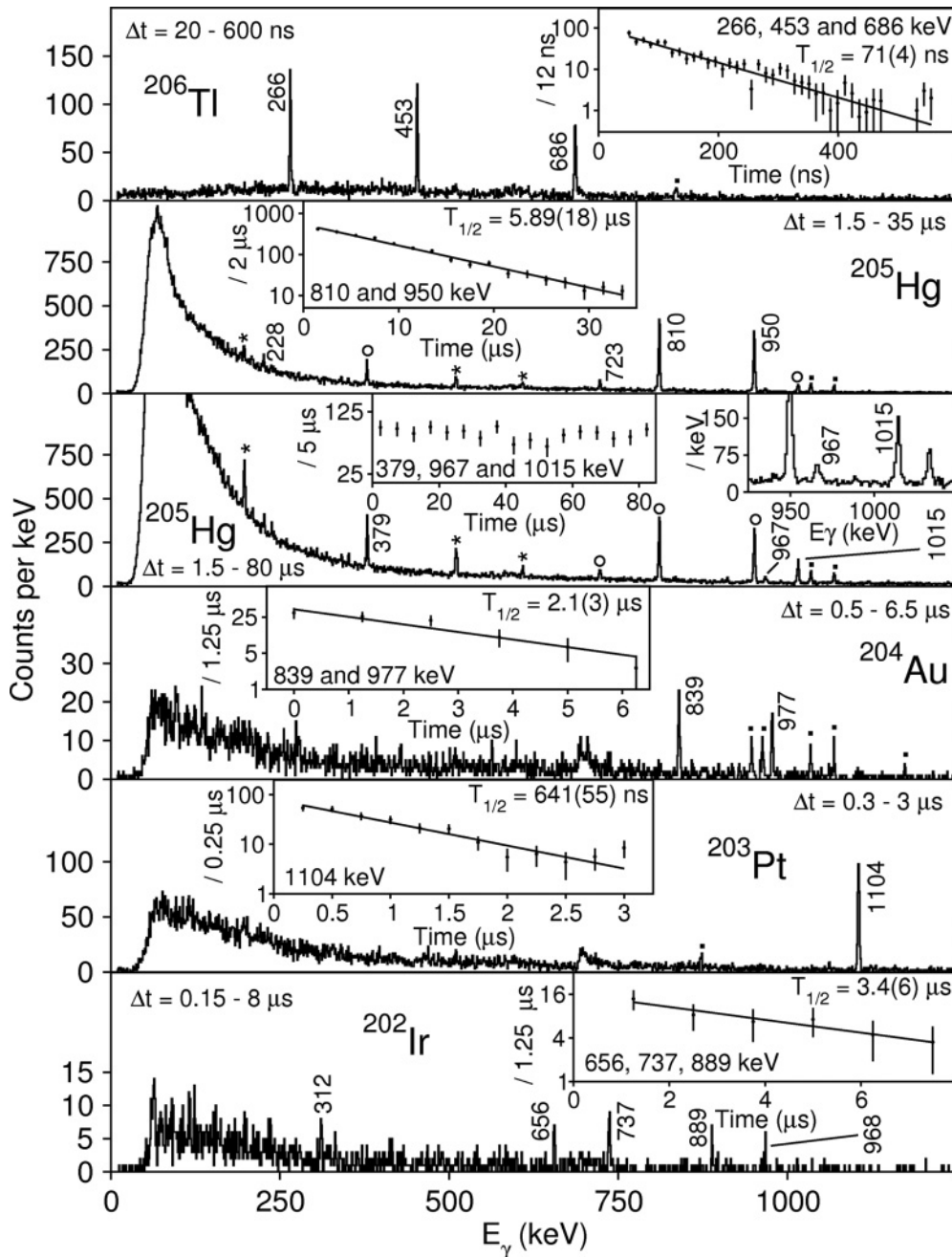
FIG. 8. Delayed γ-ray spectra for $N = 125$ nuclei. Background peaks are indicated by $\star$, transitions arising due to contaminant nuclei are indicated by, ■. The peaks indicated by ○ belong to the nucleus of interest, but originate from a different isomeric state than that for which the time limits of the γ spectrum are optimised. Inset spectra are time curves associated with the decay of the observed isomers. The transitions used to measure half-lives are indicated in the time spectra.
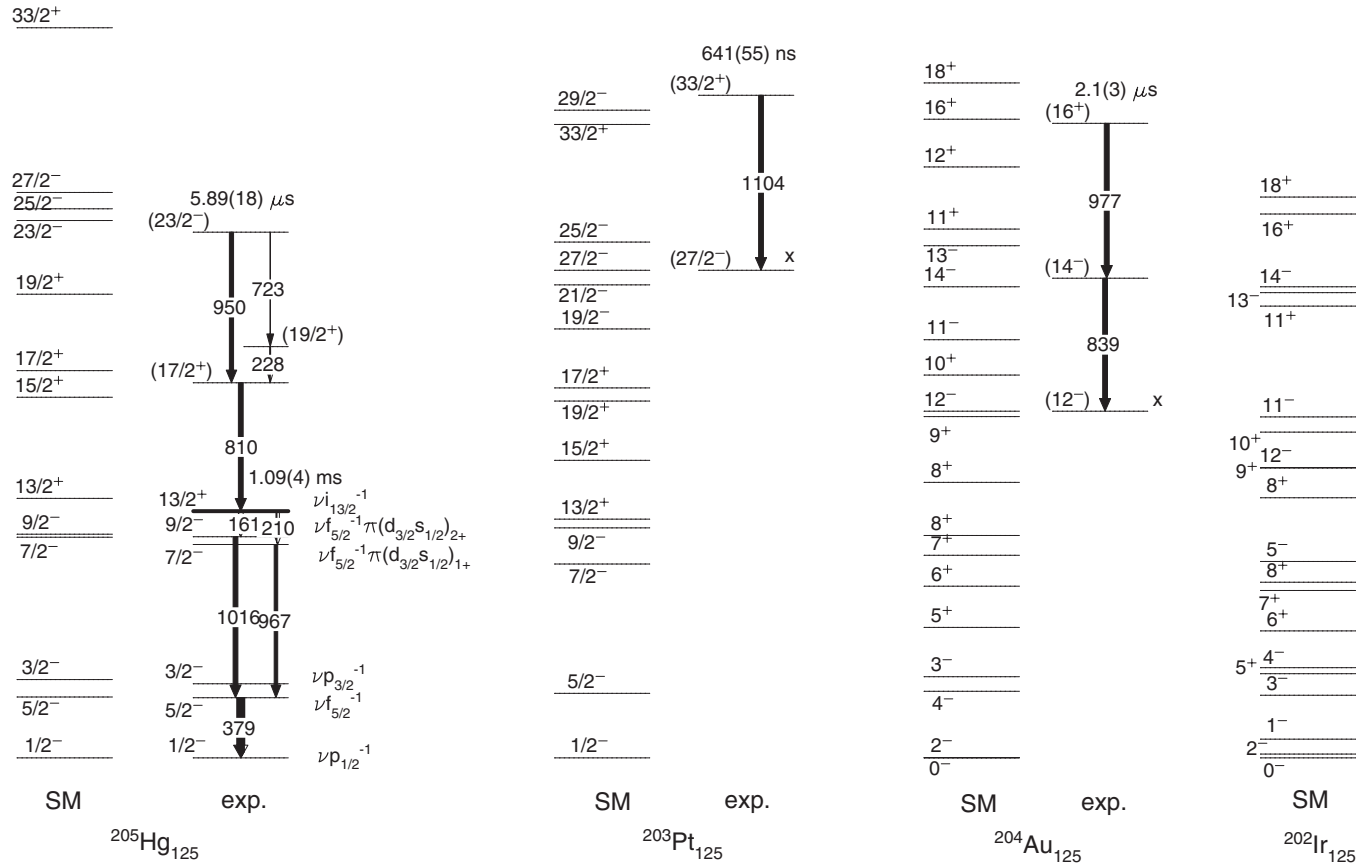
FIG. 9. Calculated and experimental level schemes for N = 125 nuclei ^{205}Hg, ^{203}Pt, ^{204}Au and ^{202}Ir. The experimental level scheme below the 13/2$^+$ isomer in ^{205}Hg, as well as its half-life is from Ref. [36].

the wave function of the final state is crucial. Analogue E3 transitions with similar transition strengths have been observed in the $N = 126$ nuclei ^{204}Pt, ^{205}Au, ^{206}Hg (see Table II), supporting our interpretation.

The level schemes of ^{203}Pt and ^{205}Hg are expected to be very similar, as shown by the calculated level schemes of Fig. 9. The obvious difference is that the negative parity three-hole states (involving the $\pi h_{11/2}$ orbital) are at lower excitation energy in ^{203}Pt, which is analogous with the ^{204}Pt–^{206}Hg case. The interpretation of the sole ^{203}Pt γ ray observed in the experiment is far from straightforward. Its submicrosecond lifetime indicates that this transition cannot be associated with the predicted $\nu i_{13/2}^{-1}$ 13/2$^+$ isomer. Similarly, the lifetime of the predicted 27/2$^-$ state ($\nu i_{13/2}^{-1}\pi h_{11/2}^{-1}d_{3/2}^{-1}$) should be much longer than the measured one and should decay through a cascade of observable transitions. Most likely the observed 1104 keV transition populates this predicted long-lived 27/2$^-$ isomeric state. The shell model suggests that the observed 1104 keV transition is the transition connecting the yrast 33/2$^+$ isomeric state with the much longer lived 27/2$^-$. The transition strength, B(E3) = 0.38(4) W.u., is in line with other octupole transitions in the region. The determined isomeric ratio of 1.3(2)% is low, as expected for high-spin isomers.

In the odd-odd ^{204}Au and ^{202}Ir nuclei, the shell model predicts isomers with spin-parity 12$^-$ and possibly 5$^+$. The 5$^+$ is expected to be very short lived, no longer than its counterpart

in ^{206}Tl with $T_{1/2} = 78$ ns (it decays via a hindered E1, and E1 transitions are forbidden in the used shell-model space). On the other hand, the 12$^-$ state with $\pi h_{11/2}^{-1}\nu i_{13/2}^{-1}$ configuration should have a much longer lifetime than the observed μs isomers, because it has to decay by E3/M4 transitions (in ^{206}Tl it has $T_{1/2} = 3.74$ min). Consequently, it is likely that the observed transitions feed the long-lived 12$^-$ isomer, again a spin trap. The observation of γ rays with similar intensity at 600–1000 keV supports this interpretation, as the 12$^-$ and 5$^+$ isomers should have very different decay patterns. In ^{204}Au, it is most likely that the two observed transitions correspond to the decay of the 16$^+$ isomer into the 14$^-$ state via an M2 + E3 and a consequent E2 into the long-lived 12$^-$ state. The ordering of the two transitions cannot be determined from the experiment and is guided by the shell model calculations. Assuming a stretched M2 decay from the 16$^+$ isomer, the transition strength is B(M2; 977 keV) = 5(1)×10^{-4} W.u.; assuming a stretched E3, the transition strength is B(E3; 977 keV) = 0.28(5) W.u. We note that the very low isomeric ratio, below 1%, supports the idea of the high-spin isomer.

In ^{202}Ir, the shell model predicts the same isomeric states and decay patterns as in its ^{204}Au isotone. Due to the larger number of observed transitions, we cannot suggest an experimental level scheme. The isomeric ratio is below 1% in this case as well, suggesting that the isomer has a high spin.
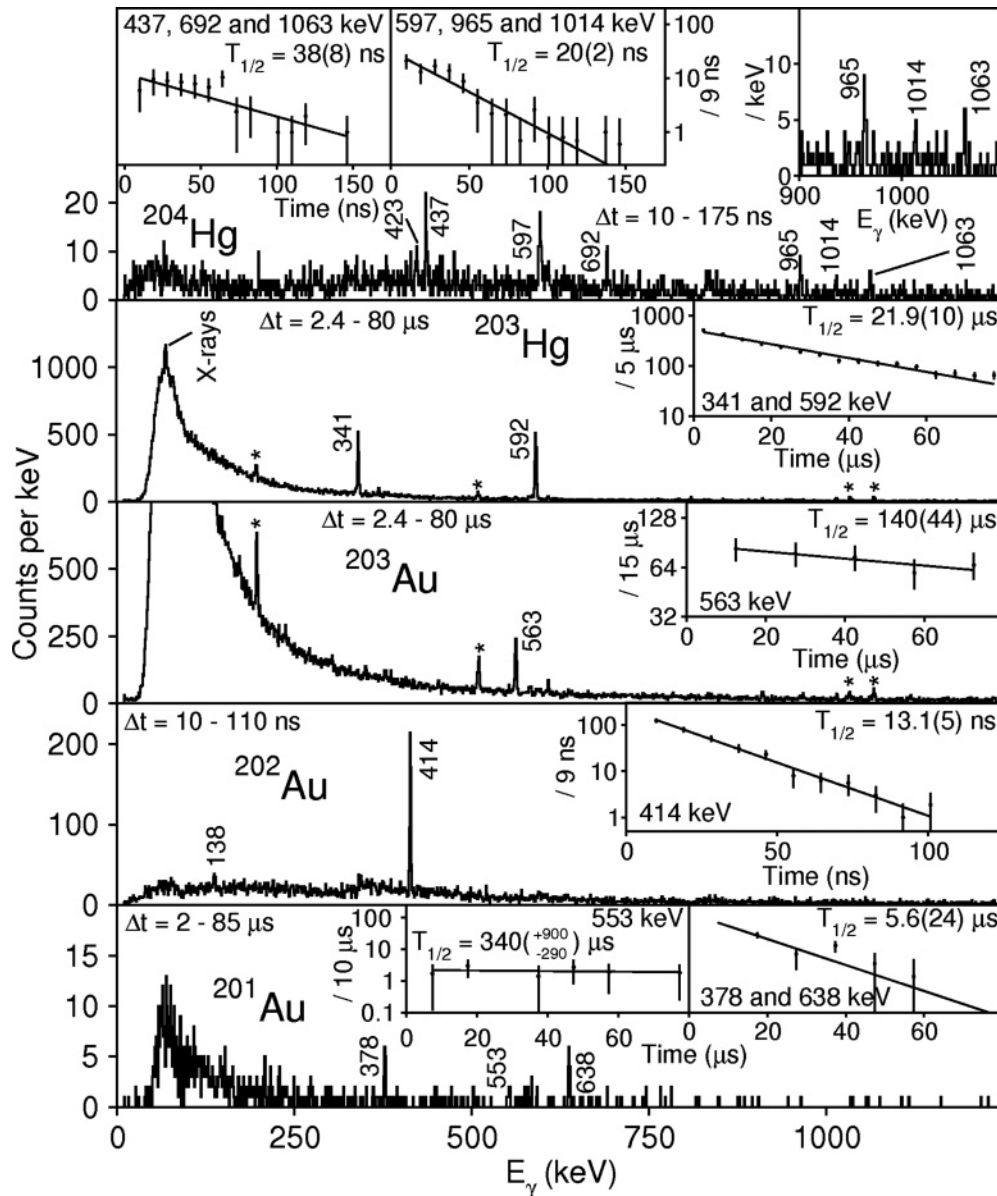
FIG. 10. Gamma-ray spectra for Hg and Au nuclei with $N < 125$ measured in the described experiment. Background peaks are indicated by ⋆. Inset spectra are time curves associated with the decay of the observed isomers. The transitions used to measure half-lives are indicated in the time spectra.

We note that the transition strengths calculated with the two shell model parametrizations are close to each other for the $N = 125$ nuclei(Table II).

D. $^{204,203}_{80}$Hg and $^{203,202,201}_{79}$Au

Delayed γ-ray spectra associated with ^{204,203}Hg and ^{203,202,201}Au are shown in Fig. 10.

In ^{204}Hg, in addition to the transitions depopulating a very short lived $I^\pi = 7^-$, $T_{1/2} = 6.7(5)$ ns [38] isomeric state, new γ lines were identified at 597, 965, and tentatively at 423 and 1014 keV (note that a 423 keV line is known to decay into the 7^- isomeric state [38]). These have equal

half-lives within experimental uncertainties, $T_{1/2} = 20(2)$ ns. The effective half-life of the transitions depopulating the 7^- isomer (437, 692, and 1063 keV) is 38(8) ns (see Fig. 10), longer than the real half-life of this metastable state. This suggests that the newly identified transitions decay into the previously known isomer. The proposed level scheme is shown in Fig. 11. Shell model calculations predict a 14^+ isomeric state decaying via a low-energy E2 transition. Due to the low statistics, we cannot establish the decay sequence from this higher-lying isomeric state.

In ^{203}Hg, the previously reported $I^\pi = (13/2^+)$ $\nu i_{13/2}^{-1}$ isomer [39] has been observed in the present work (see Fig. 11). The half-life is measured to be $T_{1/2} = 21.9(10)$ μs, which is consistent with and more accurate than the accepted value of
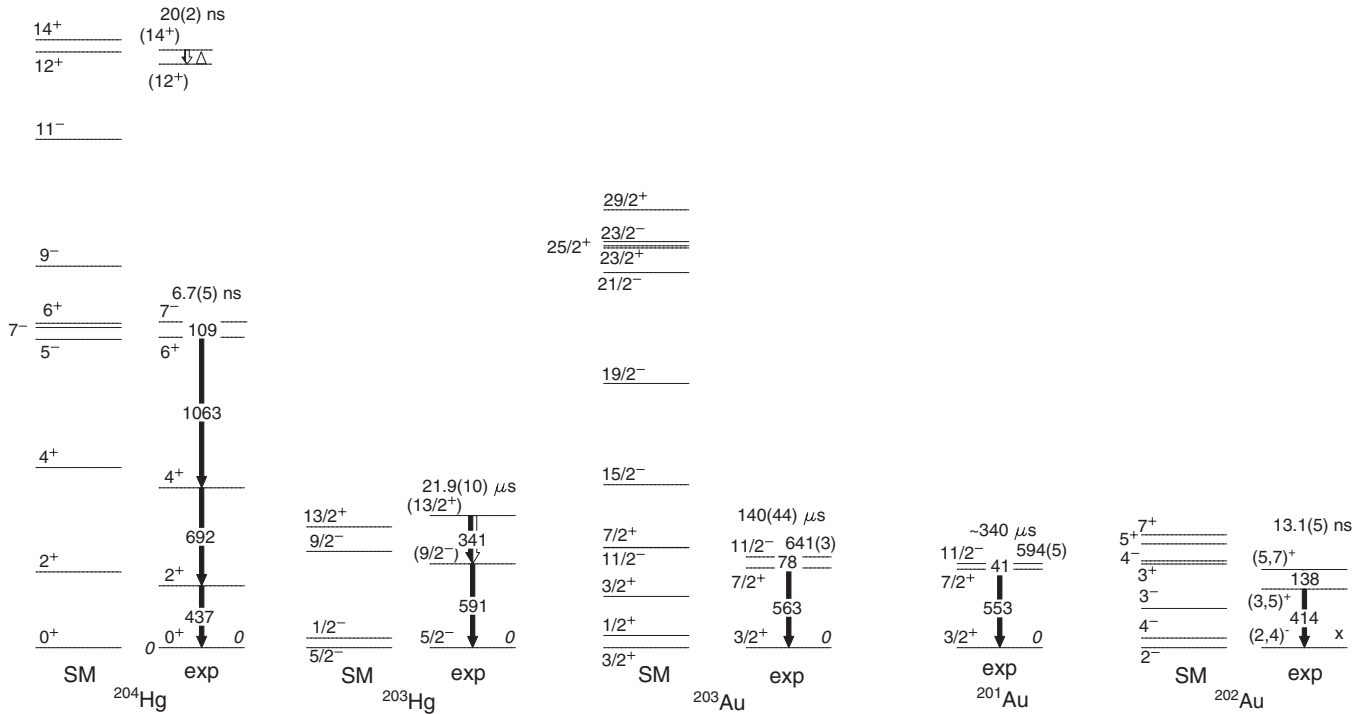
FIG. 11. Level schemes of ^{204}Hg, ^{203}Hg [39], ^{203}Au, ^{201}Au and ^{202}Au. The low-lying levels up to the 7^- isomer in ^{205}Hg [36] and the energies of the $11/2^-$ isomeric states in ^{203,201}Au [39,42] are taken from the literature.

$T_{1/2} = 24(4)$ μs. The isomer decays by an M2 transition with B(M2) = 0.0457(21) W.u. strength, which is reproduced by the shell model (see Table II).

In $^{203}_{79}$Au$_{124}$, Caamaño *et al.* [40] identified a single transition (563 keV) with a half-life of 40^{+7000}_{-20} μs. Our half-life, $T_{1/2} = 140(44)$ μs, is consistent with and more precise than the published value. The error bars are large because in this case the γ-ray correlations following implantation were limited to a maximum time of 85 μs. Nevertheless, the improved lifetime measurement is the key to the interpretation of this decay (Fig. 11). It is expected that the $\pi h_{11/2}^{-1}$ state is isomeric. A charged particle reaction experiment pinned down this state as being at 641(3) keV [38,41]. The half-life of the isomer suggests a low-energy M2 transition and rules out a low-energy E3. (Note, that while the standard shell model calculation does predict an inverse ordering of the $11/2^-$ and $7/2^+$ states, the modified one agrees with the experiment.) The observed 563 keV transition connects the $7/2^+$ state with the $3/2^+$ $\pi d_{3/2}^{-1}$ ground state. The B(M2) transition strength of the unobserved 78(3) keV γ ray is 0.03(2) W.u., in excellent agreement with the shell model prediction. The lack of strong K x rays indicates that the energy of the M2 transition is below the K-electron binding energy of 80.725 keV. The rather low isomeric ratio, 2.5^{+8}_{-10}% here and >1% in Ref. [40], suggests the existence of a higher lying long-lived isomer in this nucleus.

In $^{202}_{79}$Au$_{123}$ no excited states were reported before. Two transitions are identified at 138 and 414 keV. The half-life is $T_{1/2} = 13.1(5)$ ns. γ-γ coincidences confirmed that the two transitions are in coincidence [14]. The intensity balance supports an M1 or possible E2 assignment for the 138 keV transition. Based on the shell model calculations we propose

the tentative level scheme shown in Fig. 11. Either the 7^+ or the 5^+ state could be isomeric. The isomer decays by the 138 keV E2 transition, followed by a fast 414 keV E1. The measured transition strength, B(E2) = 5.0(2) W.u., is consistent with the ~11 W.u. value predicted by the shell model.

In ^{201}Au, three new delayed transitions are identified at 378, 553, and 638 keV. The half-life of the 553 keV transition is $T_{1/2} = 340^{+900}_{-290}$ μs, while the other two transitions originate from a shorter lived isomeric state with $T_{1/2} = 5.6(24)\mu s$. Previously, excited states of ^{201}Au were studied experimentally in the ^{202}Hg$(\vec{t},\alpha)$ reaction [41,42]. The yrast $11/2^-$ state with $\pi h_{11/2}^{-1}$ configuration was identified at 594(5) keV [42]. Below this state only low-spin states (3/2 and 1/2) and a tentative level with no spin-parity assignment at 549(5) keV were observed. Based on the lifetime, and the similarity between the observed γ-ray energy of 553 keV and the 549(5) keV excitation energy, we propose the level scheme shown in Fig. 11. The $11/2^-$ isomer at 594(5) keV decays by an unobserved low-energy 41(6) keV M2 transition into the $7/2^+$ state, which decays into the $3/2^+$ ground state by the 553 keV γ ray. This decay pattern, as well as the M2 transition strength of $B(M2) \sim 0.02$ W.u. is similar to that observed in the neighboring ^{199}Au [43] and ^{203}Au (this paper) odd-mass isotopes. This interpretation fits with the conclusions of a recent ISOLDE experiment [44]. There it was concluded [45] that the $11/2^-$ state cannot have a half-life of the order of seconds; i.e., it does not decay directly into the $3/2^-$ ground-state by an M4 transition (the case in ^{205}Au). The 638 and 378 keV transitions are associated with a higher lying isomeric state which decays into the $11/2^-$ one. The intensity balance and lifetime are compatible with the 378 keV

transition being an M2 transition decaying from the isomer with a strength of $B(M2) = 0.014(7)$ W.u. Note that due to the large number of holes outside the ^{208}Pb core, no shell model calculations were performed for ^{201}Au.

E. Platinum isotopes $^{202,201,200,199,198,197}_{78}$Pt

In $^{202}_{78}$Pt$_{124}$, an $I^\pi = (7^-)$ isomer was previously observed by Caamaño *et al.* [40]. Our half-life of $T_{1/2} = 141(7)$ μs is consistent with and more accurate than the previous value of $T_{1/2} = 280^{+420}_{-190}$ μs. γ-γ coincidence analysis has confirmed the doublet nature of the 535 keV peak [14]. This is consistent with the interpretation made by Caamaño *et al.* [40].

In $^{201}_{78}$Pt$_{123}$, the previously reported isomer [40] has been observed in the current work. In addition to the three known transitions, we searched for a possible low-energy one, without success. The isomeric half-life is measured to be $T_{1/2} = 18.4(13)$ ns, which is consistent with the previous measurement of $T_{1/2} = 21(3)$ ns [40].
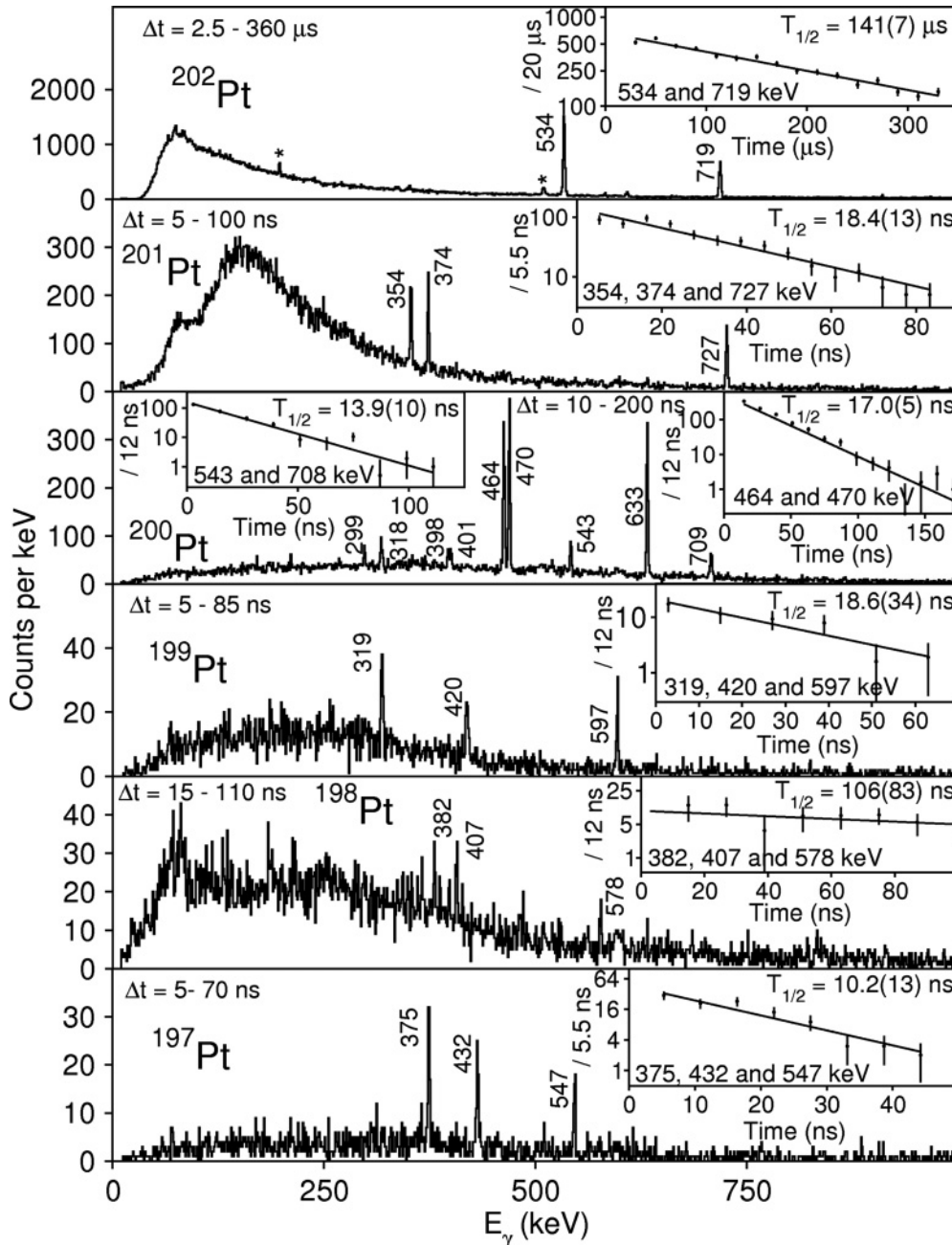
FIG. 12. Gamma-ray spectra for Pt nuclei with $N < 125$ measured in the described experiment. Background peaks are indicated by $\star$. Inset spectra are time curves associated with the decay of the observed isomers. The transitions used to measure half-lives are indicated in the spectra.
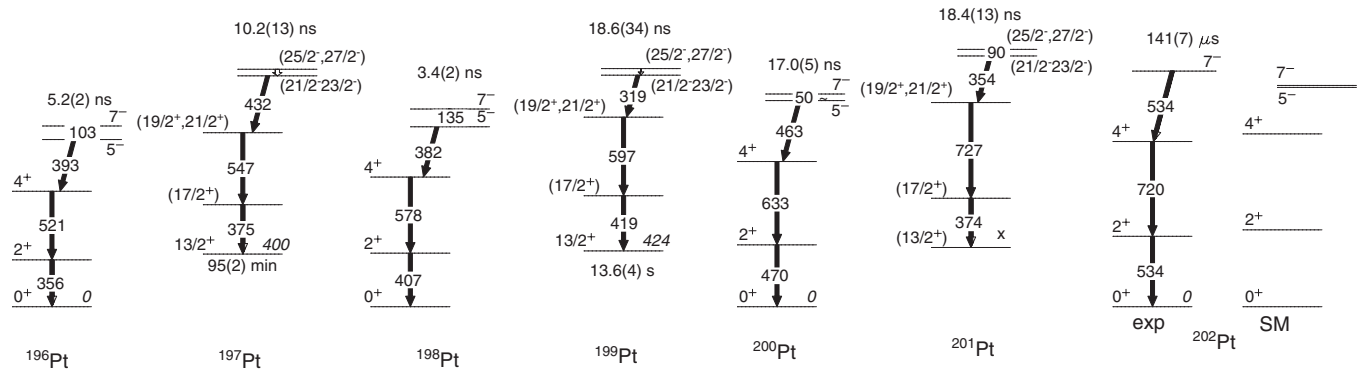
FIG. 13. Partial experimental level schemes of the $^{198-202}$Pt nuclei. The level schemes of the even-even isotopes are from [40,46,47,51,56]. The $13/2^+$ states were identified in ^{197,199}Pt before [43,54]. The half-lives are from the present work with the exception of ^{196}Pt [56] and ^{198}Pt [47]. The shell-model level scheme of ^{202}Pt is also given.

In $^{200}_{78}$Pt$_{122}$, two previously reported isomers were observed. The lower-lying $I^\pi = (7^-)$ isomer has a half-life of $T_{1/2} = 14.3(6)$ ns, which is the weighted average of the previous measurements [40,46]. This work reports a half-life of $T_{1/2} = 17.0(5)$ ns. The other isomer has only been reported by Caamaño *et al.* [40], it has a spin-parity $I^\pi = (12^+)$ and it feeds the $I^\pi = (7^-)$ isomer. The current work agrees with the previous findings and reports a half-life of $T_{1/2} = 13.9(10)$ ns; it was previously reported to be $T_{1/2} = 10.3(24)$ ns.

In $^{199}_{78}$Pt$_{121}$, we observe an unreported isomeric state. γ-ray transitions have been detected at the energies 319, 420, and 597 keV. All three transitions exhibit the same decay lifetime, within experimental uncertainties. The half-life of the isomer is $T_{1/2} = 18.6(34)$ ns.

In $^{198}_{78}$Pt$_{120}$, we observe three transitions that follow the decay of the previously reported $I^\pi = 7^-$, $T_{1/2} = 3.4(2)$ ns isomer [47]. A higher-lying isomer with $T_{1/2} = 36(2)$ ns was also reported [48,49], feeding the lower-lying $I^\pi = 7^-$ isomer. The data evaluators of Ref. [47] suggested $I^\pi = (12^-)$ for this isomer. There is weak evidence in the γ-ray energy spectrum (see Fig. 12) for the presence of the 135-, 752-, and 823-keV transitions that feed the $I^\pi = 7^-$ state; therefore, the half-life determined from the present experiment has a large uncertainty due to the poor statistics, and it is consistent with previous measurements.

In $^{197}_{78}$Pt$_{119}$, three transitions emitted following the decay of a previously unreported isomer have been detected with energies of 375, 432, and 547 keV. The three transitions are in mutual coincidence [14] and the half-life is $T_{1/2} = 10.2(13)$ ns.

The partial level schemes of the $^{196-202}$Pt nuclei are shown in Fig. 13. The even-even Pt nuclei are characterized by a 7^- isomeric state with a predominantly $\pi(h^{-1}_{11/2}d^{-1}_{3/2})7^-$ configuration. g-factor measurements [50] in lighter, $^{190-194}$Pt, isotopes support this interpretation. Due to the large number of nucleons outside the closed shell, theoretical calculations were done for ^{202}Pt only. These were performed with a truncated model space, i.e., with closed $\pi g_{7/2}$ and $\nu h_{9/2}$ orbitals. The calculations predict predominantly two-proton character for the 7^- state. (In contrast, the 7^- state in ^{204}Hg is of mixed $\pi h^{-1}_{11/2}d^{-1}_{3/2}$ and $\nu i^{-1}_{13/2}p^{-1}_{1/2}$ character.) In the case of ^{196,198,200}Pt, the 7^- isomer decays by a low-energy E2 transition into

the $\pi(h^{-1}_{11/2}s^{-1}_{1/2})5^-$ state and has a half-life of the order of nanoseconds. In the case of ^{202}Pt, the half-life is much longer, $T_{1/2} = 141(7)$ μs. This is explained by the lowering of the 7^- state below the 5^- [40,51]. The reduced transition strength is $B(E3) = 0.268(13)$ W.u. According to the interpretation proposed here, the isomers observed in the odd-mass Pt isotopes have similar structure to that in the neighboring even-even Pt isotopes, with an added neutron in the $i_{13/2}$ orbital. Isomeric states with similar structure were previously identified in lighter Pt isotopes, such as ^{191,193}Pt [52,53]. This interpretation differs from the previously suggested one [40] for ^{201}Pt (the data on the isomers in ^{197,199}Pt is new). Previously, it was proposed that the isomer populates the $5/2^-$ ground state. The present interpretation is based on the similarities between the isomers observed in these nuclei: there are always three strong transitions in similar energy regimes; and the half-lives are of the order of tens of nanoseconds (with the exception of ^{202}Pt). The scenario is also supported by the E2 strengths, which for ^{200}Pt is $\sim$13 W.u. close to the value of 11 W.u. calculated for ^{202}Pt, the last one accessible to shell model calculations. With increasing distance from $N = 126$ an increase to twice this value is observed for both the even-A and odd-A isotopes.

We note that the $13/2^+$ state is known in ^{197}Pt [54] and ^{199}Pt [43] but was not observed in ^{201}Pt. The ordering of the three transition in the odd-mass nuclei is based on the systematics. The exception is the $17/2^+$ state in ^{197}Pt, where a $(17/2^+)$ state at 767(10) keV was previously identified in a $(^3$He,$\alpha)$ reaction [54,55].

F. Iridium isotopes $^{201,200,199,198,195}_{77}Ir_{124}$

The delayed γ-ray and time spectra of $^{201,200,199,198,195}_{77}Ir_{124}$ are shown in Fig. 14.

In $^{201}_{77}$Ir$_{124}$, no experimental information on the excited states was previously available. Presently, an isomer has been observed, emitting three transitions: 440, 452, and 681 keV. The half-life is $T_{1/2} = 10.5(17)$ ns.

No experimental information on the excited states of $^{200}_{77}$Ir$_{124}$ was previously available. Two transition were
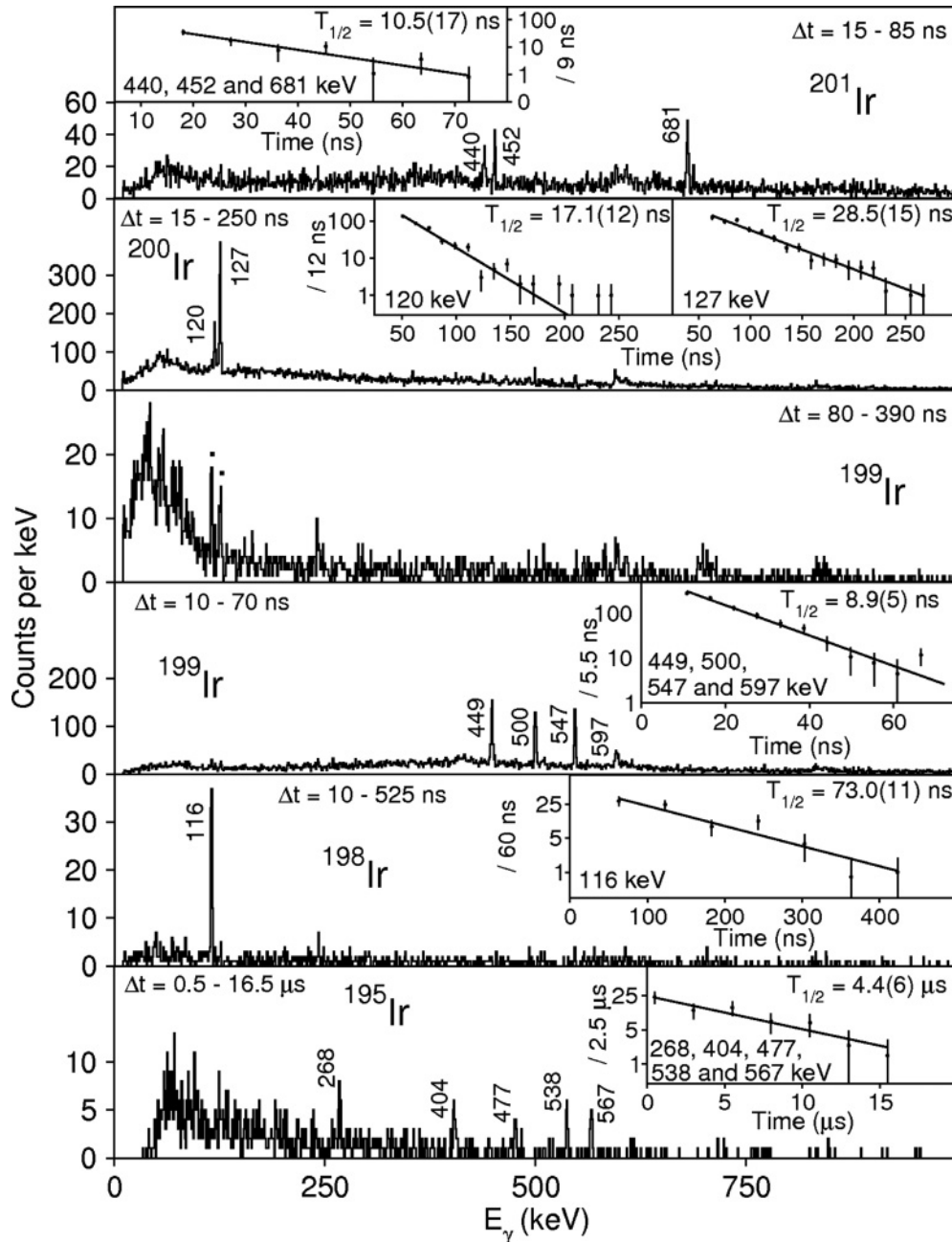
FIG. 14. Gamma-ray spectra for Ir nuclei with $N < 125$ measured in the described experiment. Transitions arising from contaminant nuclei are indicated by, ∎. Inset spectra are time curves associated with the decay of the observed isomers. The transitions used to measure half-lives are indicated in the spectra.

observed, at energies of 120 and 127 keV. The transitions are not in coincidence with each other [14]. The half-lives associated with the decay of these two transitions are $T_{1/2} =$ 17.1(12) and 28.5(15) ns, respectively.

In $^{199}_{77}\mathrm{Ir}_{122}$, a new isomeric state has been observed decaying by 449-, 500-, 547-, and possibly 597-keV transitions. The intensity of the tentative 597-keV transition (its energy is similar to that from the $^{74}\mathrm{Ge}(n,n')$ reaction) is distinctly less than the intensity of the other three. γ-γ coincidence analysis shows that the three stronger transitions are in mutual coincidence. In addition, the 500 keV is a doublet, since

it is in coincidence with itself. The 597-keV transition is tentatively observed to be in coincidence with the other three transitions. Based on the presently available experimental data, it is interpreted that all of the transitions are emitted following the decay of a single isomer with a half-life of $T_{1/2} = 8.9(5)$ ns. Caamaño *et al.* [40] have previously tentatively reported the existence of an isomer in $^{199}_{77}\mathrm{Ir}_{122}$. Candidate transitions were suggested at the energies 104, 112, 122, and 162 keV. Our spectrum, with the same time range $\Delta t = 80 \rightarrow 390$ ns is shown in Fig. 14. No indication of the tentatively observed isomer has been detected in this work.
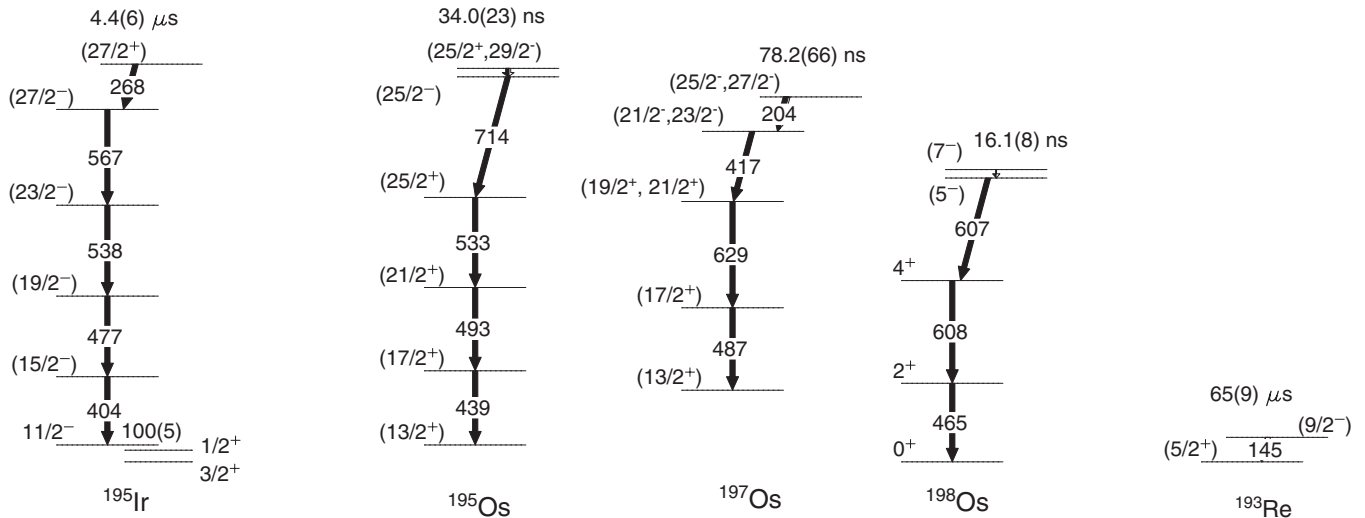
FIG. 15. Tentative level schemes for iridium, osmium and rhenium isotopes. The single particle states in ^{195}Ir are from literature [54,57]. For a more complete level scheme of ^{198}Os see [58].

An isomer has previously been identified in $^{198}_{77}$Ir$_{121}$ with a half-life of $T_{1/2} = 77(9)$ ns [40]. Our measured half-life of $T_{1/2} = 73.0(11)$ ns is in agreement with the previous value.

A previously unreported isomer has been identified in $^{195}_{77}$Ir$_{118}$. The transitions are observed to have energies 268, 404, 477, 538, and 567 keV. None of these transitions were known before [57]. The half-life of the isomer measured from the combined statistics of all of the transitions is found to be $T_{1/2} = 4.4(6)$ μs.

The odd-mass ^{193,195,197}Ir nuclei have a remarkably similar single quasiparticle level structure [53,54,57]. The ground-state is $\pi 3/2^+[402]$, followed by the $\pi 1/2^+[400]$ at ~60-keV excitation energy and by $\pi 11/2^-[505]$ at ~100 keV. The $11/2^-$ is isomeric with very long half-life (e.g., 10.5 days in ^{193}Ir). The similarity indicates that these isotopes must have very similar deformation. This, and the further similarity to less neutron-rich ^{189,191}Ir nuclei suggests that they all exhibit prolate deformation (note that the calculations of Möller *et al.* [29] suggest that Ir isotopes up to ^{196}Ir are prolate, and become oblate from ^{197}Ir onwards). The proposed level scheme for ^{195}Ir is shown in Fig. 15. Based on BCS calculations, we suggest for ^{195}Ir that a three-quasiparticle $27/2^+$ isomer with configuration $\pi 11/2^-[505]\nu 3/2^-[512]13/2^+[606]$ decays into the rotational band built on $\pi 11/2^-[505]$. The transition energies within the band fit into the systematics of the lighter odd-mass Ir isotopes. The transition strength of the 268-keV E1 transition is B(E1) = $2.3(3)\times10^{-9}$ W.u.

In ^{198}Ir and ^{200}Ir, the lack of x rays in the spectra suggests that the observed low-energy transitions are of E1 character. In the case of ^{198}Ir, following the previous suggestion [40] that the observed transition is E1 in nature and it depopulates the isomer directly, a transition strength of B(E1) = $1.4(3)\times10^{-6}$ W.u. and an isomeric ratio of IR = 5(4)% is measured. This is lower than the previous IR = 19^{+5}_{-3} value [40]. With the same assumptions for ^{200}Ir, we get

B(E1) = $2.8(2)\times10^{-6}$ W.u and B(E1) = $5.4(4)\times10^{-6}$ W.u, IR = 3.5(14)% and IR = 22(12)%, for the 127- and the 121-keV transitions, respectively.

The lifetimes, of order of tens of nanoseconds, in ^{201}Ir and ^{199}Ir are compatible with decays via low-energy E2 transitions. Both nuclei are predicted to be almost spherical, with small, $\beta_2 < 0.1$, oblate deformation [29]. The observed γ-ray spectra do not resemble rotational bands, in agreement with the above prediction. No level schemes are proposed for these nuclei.

G. Osmium isotopes $^{199,198,197,195,193}_{77}$Os

The delayed γ-ray and time spectra for $^{199,198,197,195,193}_{77}$Os nuclei are shown in Fig. 16.

A previously unreported isomer has been observed in ^{199}Os. Five transitions have been detected with energies 379, 402, 425, 737, and 971 keV. The half-life of the isomer is measured to be $T_{1/2} = 25.2(20)$ ns.

Two new isomers were found in $^{198}_{76}$Os$_{122}$. These results have been discussed in detail by Podolyák *et al.* [58]. In supplement to the previous publication, we present here limits on the isomeric ratios of the observed $I^\pi = (12^+)$ and (7^-) metastable states (see Table I).

No states have previously been reported in $^{197}_{76}$Os$_{121}$. Presently, four transitions have been observed, these are at energies 204, 416, 487, and 629 keV. The half-life is found to be $T_{1/2} = 78.2(66)$ ns. All four transitions are in mutual coincidence [14].

In $^{195}_{76}$Os$_{119}$, we confirm the isomeric state previously observed both in fragmentation [40] and deep-inelastic [48] experiments. Our half-life is $T_{1/2} = 34.0(23)$ ns, similar to the previously determined values of $T_{1/2} = 26(4)$ ns [40] and $T_{1/2} = 26(9)$ ns [48].

An isomer is reported for the first time in ^{193}Os$_{117}$. One transition with 242 keV is associated with the decay of the isomer that has a half-life of $T_{1/2} = 132(29)$ ns. This energy does not fit into the known low-spin-level scheme [53] and we are unable to propose a level scheme.

The observed isomer in ^{195}Os was interpreted [48] to have $I^\pi = (27/2^-)$ with $\nu 13/2^+[606]3/2^-[501]11/2^+[615]$ character. Here we suggest an alternative interpretation, as shown in Fig. 15. The $I^\pi = (29/2^-)$ with $\nu 13/2^+[606]\pi 11/2^-[505]5/2^+[402]$ (or, alternatively, the $I^\pi = (25/2^+)$ with $\nu 13/2^+[606]3/2^-[501]9/2^-[505]$) isomer decays via a low-energy E2 (or E1) transition into the $25/2^-$, $\nu 13/2^+[606]11/2^-[505]1/2^+[411]$ band-head, which decays via the 714-keV transition into the $\nu 13/2^+[606]$ band. We note that the $\nu 13/2^+[606]$ and $\nu 3/2^-[501]$ states are expected to be close in energy, one of them being the ground state and the other a long-lived isomer.

Theoretical calculations predict a weakly deformed oblate shape for $^{197-199}$Os [29,59], similar to the platinum isotopes. From the experimental side, the similarity between the excitation spectra of ^{198}Os and ^{200}Pt [58] suggests that the neighboring odd-mass nuclei are also similar. Consequently, a low-energy $13/2^+$ state, with a long half-life, is expected in the odd-mass Os isotopes. Most likely, the isomers observed in ^{197,199}Os decay into this yrast $13/2^+$ state. Possible isomeric states should have the $i_{13/2}$ neutron coupled with $\pi h_{11/2}^{-1}d_{3/2}^{-1}$ and/or $\pi h_{11/2}^{-2}$. For ^{197}Os, we suggest a level scheme similar to that of its ^{199}Pt isotone, with the isomer having $\nu i_{13/2}^{-1}\pi h_{11/2}^{-1}d_{3/2}^{-1}$ configuration (see Figs. 15 and 13). In ^{199}Os, the number of observed γ rays suggests a higher spin isomer, possibly with $\nu i_{13/2}^{-1}\pi h_{11/2}^{-2}$ character; however, we are unable to propose a level scheme.

We note that no isomeric state was observed in ^{196}Os [58]. This suggests that ^{196}Os has a different shape from the slightly
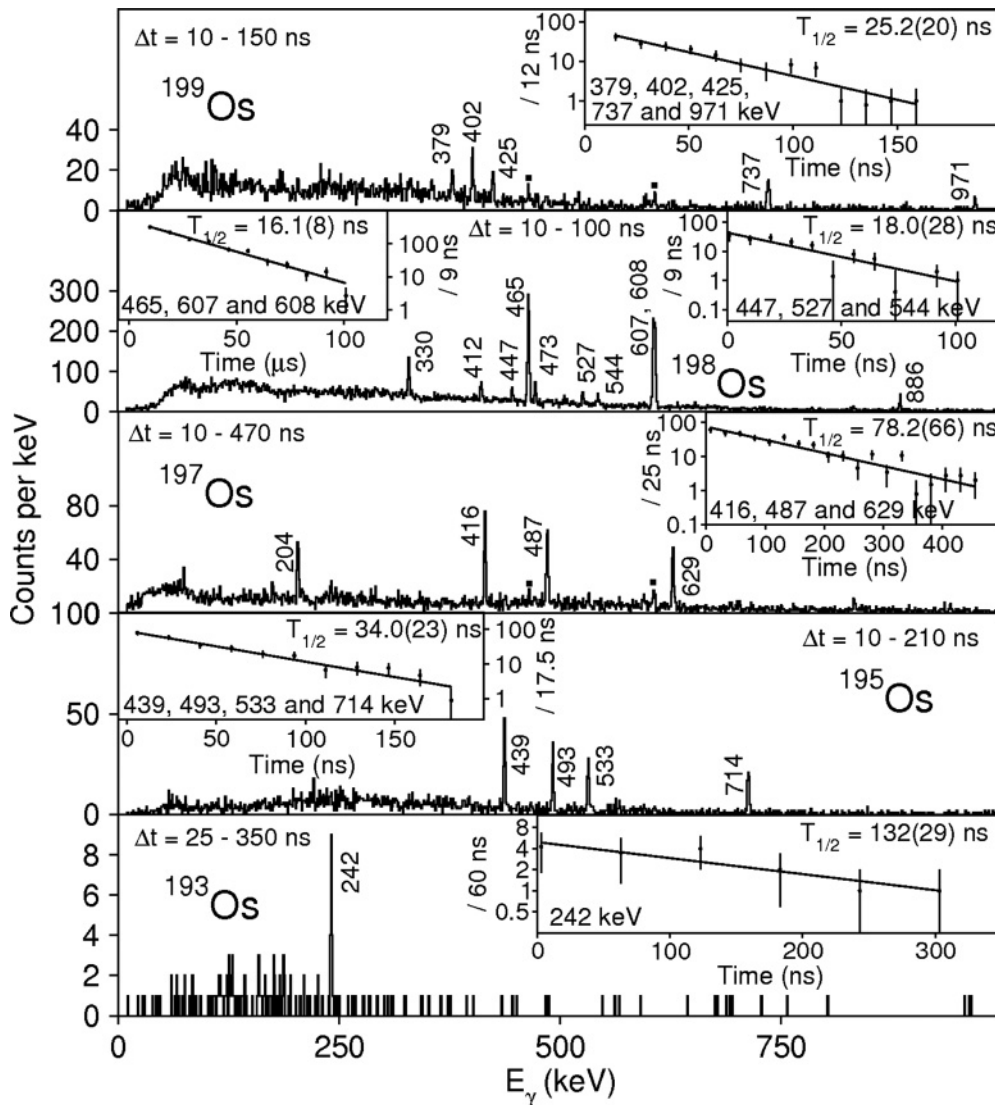

FIG. 16. Gamma-ray spectra for Os nuclei measured in the described experiment. Inset spectra are time curves associated with the decay of the observed isomers. The transitions used to measure half-lives are indicated in the spectra.
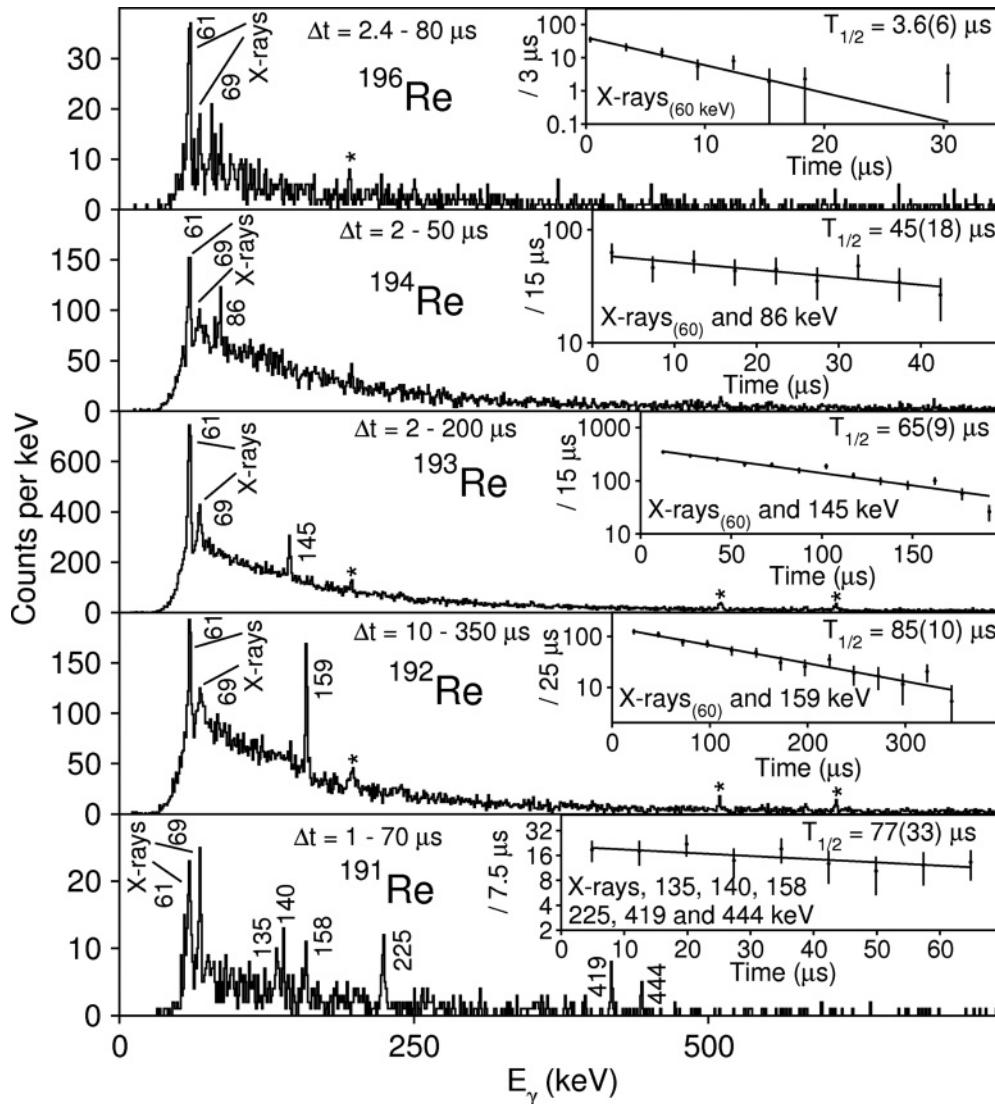
FIG. 17. Gamma-ray spectra for Re nuclei measured in the described experiment. Background peaks are indicated by $\star$. Inset spectra are time curves associated with the decay of the observed isomers. The transitions used to measure half-lives are indicated in the spectra.

oblate ^{198}Os [58] and the platinum isotopes. Here we propose that the shape transition to oblate happens after ^{196}Os.

H. Rhenium isotopes $^{196,194,193,192,191}_{75}$Re

The delayed γ-ray and time spectra of $^{196,194,193,192,191}_{75}$Re nuclei are shown in Fig. 17.

For the first time an excited state is reported to be observed to decay in ^{196}Re. Characteristic rhenium K_α and K_β x rays are observed following the decay through an unobserved highly converted transition. The half-life associated with the K_α x rays is measured to be $T_{1/2} = 3.6(6)$ μs.

In $^{194}_{75}$Re$_{119}$, Caamaño *et al.* [40] tentatively reported an isomeric state by observing possible transitions at 128, 148, and 464 keV and rhenium K_α and K_β x rays. The current report confirms the existence of an isomer with a measured half-life of $T_{1/2} = 45(18)$ μs. We observe the x rays and the

86-keV γ ray. The 128-, 148-, and 464-keV transitions have not been observed.

In ^{193}Re previous work by Caamaño *et al.* [40] identified the emission of a 145-keV γ-ray transition and characteristic rhenium K_α and K_β x rays following the decay of an isomer with a half-life of $T_{1/2} = 75^{+300}_{-40}$ μs. We confirm the existence of this isomer. The determined half-life, $T_{1/2} = 65(9)$ μs, is consistent with and more precise than the previous value. A more recent experiment also detected this isomer and gave $T_{1/2} = 72(8)$ μs [60].

In $^{192}_{75}$Re$_{117}$ Caamaño *et al.* [40] have previously identified the decay of an isomer. We confirm the existence of this isomer by detecting a 159 keV, γ ray, as well as characteristic rhenium K_α and K_β x rays. The determined half-life, $T_{1/2} = 85(10)$ μs, is consistent with and more precise than the previous value of $T_{1/2} = 120^{+210}_{-50}$ μs. A more recent experiment also detected this isomer and reported $T_{1/2} = 93(15)$ μs [60].

In $^{191}_{75}$Re$_{116}$, an isomer has tentatively been identified by Caamaño *et al.* [40] with possible transitions at 53, 139, 225, 308, 360, 419, and 444 keV with Re x rays as well. We confirm the existence of this isomer. There are differences between the transitions observed in this and the previous work. The suggested transitions at 53, 308, and 360 keV have not been observed in this work, although the others have. In addition, in this work a transition of 135 keV is tentatively identified, which was not previously observed. The intensity of the 225-keV line is double compared to the others, suggesting a doublet nature. The half-life of the isomer is $T_{1/2} = 77(33)$ μs.

Odd-mass ^{187}Re [61] and ^{189}Re [61] are characterized by an $\pi 5/2^+$[402] ground state with a low-lying $\pi 9/2^-$[514] excited state. Our BCS calculations predict the same situation for ^{193}Re. We propose that the observed 145-keV transition connects these states and has an M2 transition strength of $B(M2) = 0.0175(25)$ W.u. The intensity of the observed x rays is in agreement with this scenario.

In ^{191}Re, we are unable to suggest a level scheme. Most likely the isomer feeds the $\pi 9/2^-$[514] band head as the energy of the 140-keV transition is in agreement with the $(11/2^-) \rightarrow (9/2^-)$ energy difference [52]. The strong x rays as well as the lifetime suggest an M2 decay from the isomer, possibly arising from the same proton configuration change (with a broken neutron pair) as in ^{193}Re. We note that the $9/2^-$ band head at 145(3) keV [52] is likely to be isomeric with a similar lifetime, decaying into the $5/2^+$ band head at 97(3) keV (but the observed x rays are not from this decay and the 97(3)-keV transition is not observed).

The odd-odd ^{192,194,196}Re nuclei all exhibit strong x rays and similar microseconds lifetimes. These would suggest a low-energy M2 decay, similarly to the odd-mass nuclei. However, the x rays in ^{192}Re and ^{194}Re are too weak for the 159- and 86-keV transitions to be of M2 character, respectively. Consequently, no level schemes are suggested for the odd-odd rhenium nuclei. The isomeric ratios were determined assuming M1 character for the 159- and 86-keV transitions.
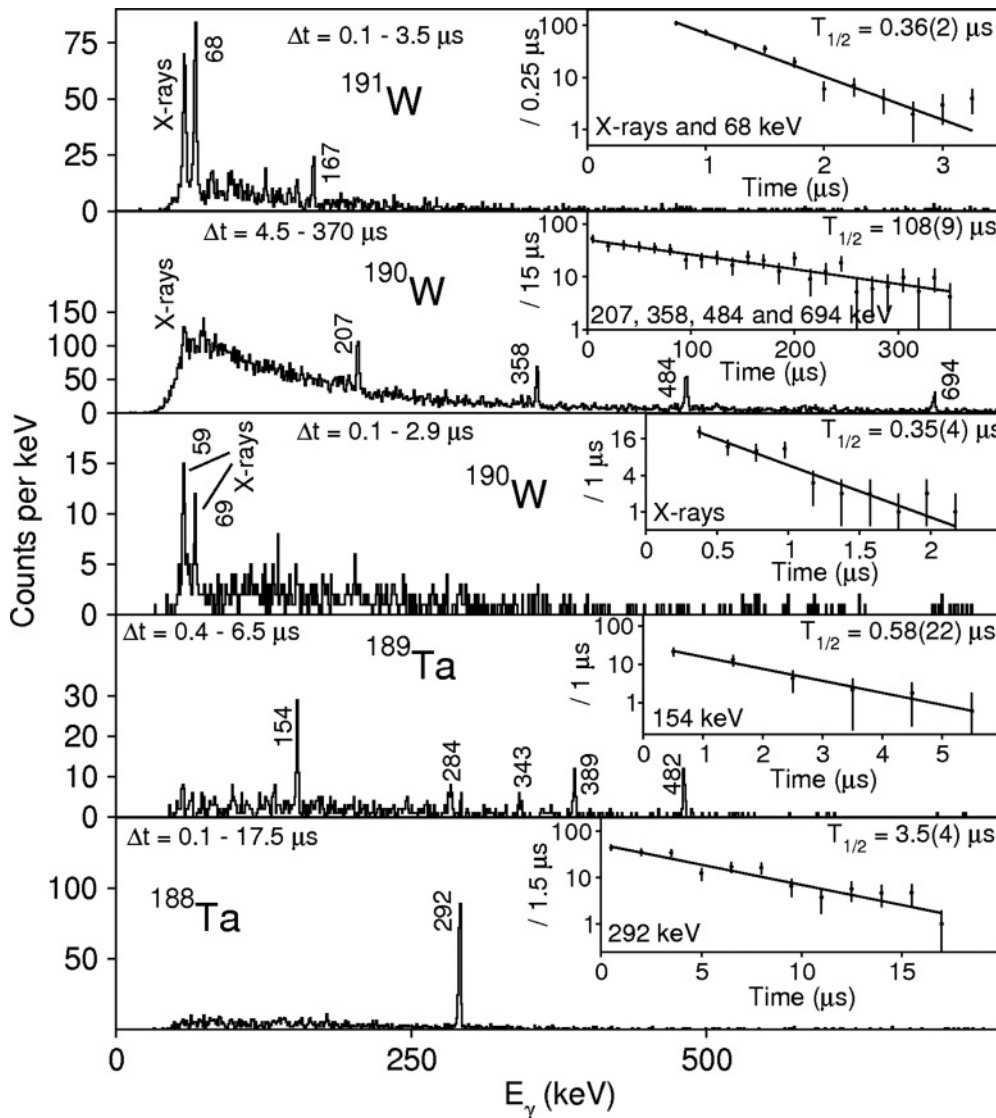

FIG. 18. Gamma-ray spectra for W and Ta nuclei measured in the described experiment. Inset spectra are time curves associated with the decay of the observed isomers. The transitions used to measure half-lives are indicated in the spectra.

I. The $^{191,190}_{74}$W and $^{189,188}_{73}$Ta nuclei

The delayed γ-ray and time spectra of ^{191,190}W and ^{189,188}Ta nuclei are shown in Fig. 18.

The first observation of excited states in $^{191}_{74}$W have been made in the present work [13,14]. γ-ray transitions at 68 and 167 keV and characteristic tungsten x rays are observed. The half-life is $T_{1/2} = 0.36(2)$ μs. This isomer is confirmed by Alkhomashi *et al.*, who in a subsequent experiment performed one year later measured $T_{1/2} = 0.32(2)$ μs [60]. We are unable to propose a level scheme.

In $^{190}_{74}$W$_{114}$, an isomeric state has been previously reported [40,62]. The results from the present experiment and possible interpretations were discussed in detail in Ref. [63]. The half-life of the isomer has been measured to be $T_{1/2} = 108(9)$ μs. We note that a subsequent experiment confirmed this isomer and reported a half-life of $T_{1/2} = 106(18)$ μs [60]. In addition, there are indications for a previously unreported isomer with a much shorter life-time. Characteristic tungsten x rays have been observed, but no γ-ray transitions, with an associated half-life of $T_{1/2} = 0.35(4)$ μs. There are insufficient statistics available for γ-γ analysis to identify whether there is any feeding between this newly discovered isomer and the previously observed one. Very recently, results from an experiment employing deep-inelastic collisions were published by Lane *et al.* [64]. They deduce that a 10^- $T_{1/2} = 166(6)$ μs isomer decays by a low-energy M2 transition into the 8^+ 110(17) ns isomer. The lower-lying isomer decays via the γ-ray transitions observed in the present experiment. Our experimental data supports the level scheme suggested by Lane *et al.* (see Fig. 1 of Ref. [64]). However, our short-lived x-ray spectrum cannot be explained by that level scheme. It was previously noted that a possible cause of the low E(4$^+$)/E(2$^+$) ratio in ^{190}W is shape coexistence [9]. Consequently, it might be that the observed x rays are from the $0^+ \rightarrow 0^+$ shape-changing transition. This has to be isomeric also because its decay has to proceed via conversion electron as the γ-ray transition is forbidden.

Excited states have been measured in $^{189}_{73}$Ta$_{116}$ for the first time. γ-ray transitions have been observed at energies of 154, 284, 343, 389, and 482 keV. The half-life is $T_{1/2} = 0.58(22)$ μs. γ-γ coincidence analysis shows that all of the γ rays are in mutual coincidence [14]. A more recent experiment has also detected this isomer. γ rays with energies 57 (x ray), 83, 134, 154, 199, 264, 284, 389, and 481 keV were reported with a half-life of $T_{1/2} = 1.6(2)$ μs [60]. The additional, lower intensity γ rays show up in our spectrum as tentative lines (also 99 keV). It seems that two isomers are involved, and we are unable to propose a level scheme

In $^{188}_{73}$Ta$_{115}$, we confirm the previous observation of an isomeric state by Caamaño *et al.* [40]. A single 292-keV transition is observed with half-life of $T_{1/2} = 3.5(4)$ μs, which is in agreement with the previous value of $T_{1/2} = 5(2)$ μs.

A subsequent fragmentation experiment has also seen this isomer and reported a $T_{1/2} = 4.4(10)$ μs half-life [60]. No level scheme is proposed.

J. Lighter nuclei

The experiment covered a number of nuclei in the $Z = 69-72$ (Tm-Hf) region, as shown in Fig. 5. The yields of these nuclei were rather low [13]. Therefore, no conclusion can be drawn from the nonobservation of isomeric states in the region. To some extent, the above is valid for tantalum isotopes as well. Actually, we know that this region is characterized by K isomerism, and some K isomers have been identified. For example, fragmentation experiments populate isomeric states in ^{190}Ta [60] and ^{183,184,186}Hf [65], while deep-inelastic reactions made them in ^{182}Hf [66].

IV. SUMMARY

Isomeric states were observed in a large number of heavy neutron-rich nuclei in the Ta-Hg region. In the case of nuclei close to the doubly magic ^{208}Pb, the results were interpreted with the aid of the shell-model. It was found that the modifications introduced in order to obtain a better description of ^{204}Pt and ^{206}Hg improved the agreement with experiment for the whole region.

Information on the prolate-oblate shape transition was obtained. It is suggested that osmium isotopes with mass $A \geqslant 197$ are slightly oblate and have isomeric states similar to those in the platinum nuclei. The lighter osmium isotopes such as ^{193,195}Os exhibit isomeric states characteristic of prolate shapes. The lack of isomeric transitions in ^{196}Os are interpreted as an indication that this nucleus is still prolate deformed. The spectra obtained from iridium isotopes indicate that up to ^{197}Ir they are prolate while the ^{199,201}Ir isotopes are oblate.

Several isomeric states with half-lives beyond the sensitivity of the technique used here are predicted. It may be possible to identify them using other methods, such as the GSI storage ring.

[1] J. H. D Jensen, Rev. Mod. Phys. **29**, 182 (1957).

[2] D. Eccleshall and M. J. L. Yates, Phys. Lett. **19**, 301 (1965).

[3] J. A. Becker *et al.*, Phys. Rev. C **26**, 914 (1982).

[4] K. H. Maier *et al.*, Phys. Rev. C **30**, 1702 (1984).

[5] B. Fornal *et al.*, Phys. Rev. Lett. **87**, 212501 (2001).

[6] Ch. Wennemann *et al.*, Z. Phys. A **347**, 185 (1994).

[7] K. Nomura *et al.*, Phys. Rev. C **83**, 054303 (2011).

[8] P. Sarriguren, R. Rodriguez-Guzman, and L. M. Robledo, Phys. Rev. C **77**, 064322 (2008).

[9] P. D. Stevenson, M. P. Brine, Z. Podolyak, P. H. Regan, P. M. Walker, and J. R. Stone, Phys. Rev. C **72**, 047303 (2005).

[10] S. Pietri *et al.*, Nucl. Instrum. Methods Phys. Res., Sect. B **261**, 1079 (2007).

[11] H. Geissel *et al.*, Nucl. Instrum. Methods Phys. Res., Sect. B **70**, 286 (1992).

[12] S. Pietri *et al.*, Acta Phys. Pol. **38**, 1255 (2007).

[13] S. J. Steer *et al.*, Int. J. Mod. Phys. E **18**, 1002 (2009).

[14] S. J. Steer, Ph.D. Thesis, University of Surrey, unpublished (2008).

[15] S. Myalski *et al.*, Acta Phys. Pol. B **40**, 879 (2009).

[16] Zs. Podolyák *et al.*, Eur. Phys. J. Special Topics **150**, 165 (2007).

[17] Zs. Podolyák *et al.*, Phys. Lett. B **632**, 203 (2006).

[18] C. Scheidenberger *et al.*, Nucl. Instrum. Methods Phys. Res., Sect. B **142**, 441 (1998).

[19] S. J. Steer *et al.*, Phys. Rev. C **78**, 061302(R) (2008).

[20] Zs. Podolyák *et al.*, Eur. Phys. J. A **42**, 489 (2009).

[21] Zs. Podolyák *et al.*, Nucl. Phys. A **722**, 273c (2003).

[22] P. Detistov, D. L. Balabanski, and Zs. Podolyák, Acta Phys. Pol. B **38**, 1287 (2007).

[23] M. Pfützner *et al.*, Phys. Rev. C **65**, 064604 (2002).

[24] B. A. Brown *et al.*, MSU-NSCL report 1289 (2004).

[25] L. Rydström, J. Blomqvist, R. J. Liotta, and C. Pomar, Nucl. Phys. A **512**, 217 (1990).

[26] T. T. S. Kuo and G. H. Herling, US Naval Research Laboraotory, Report No. 2258, unpublished (1971).

[27] H. Grawe, K. Langanke, and G. Martínez-Pinedo, Rep. Prog. Phys. **70**, 1525 (2007).

[28] K. Jain *et al.*, Nucl. Phys. A **591**, 61 (1995).

[29] P. Moller, J. R. Nix, W. D. Myers, and W. J. Swiatecki, At. Data Nucl. Data Tables **59**, 185 (1995).

[30] F. G. Kondev, Nucl. Data Sheets **109**, 1527 (2008).

[31] E. C. Simpson, J. A. Tostevin, Zs. Podolyák, P. H. Regan, and S. J. Steer, Phys. Rev. C **80**, 064608 (2009).

[32] E. C. Simpson, J. A. Tostevin, Zs. Podolyák, P. H. Regan, and S. J. Steer, Phys. Rev. C **82**, 037602 (2010).

[33] R. Kumar *et al.*, Nucl. Instrum. Methods Phys. Res., Sect. A **598**, 754 (2009).

[34] Zs. Podolyák *et al.*, Phys. Lett. B **672**, 116 (2009).

[35] O. Häusser, J. R. Beene, T. K. Alexander, A. B. McDonald, and T. Feastermann, Phys. Lett. B **64**, 273 (1976).

[36] F. G. Kondev, Nucl. Data Sheets **101**, 521 (2004).

[37] A. I. Morales *et al.*, Acta Phys. Pol. B **40**, 867 (2009).

[38] C. J. Chiara and F. G. Kondev, Nucl. Data Sheets **111**, 141 (2010).

[39] F. G. Kondev, Nucl. Data Sheets **105**, 1 (2005).

[40] M. Caamaño *et al.*, Euro. Phys. J. A **23**, 201 (2005).

[41] E. R. Flynn *et al.*, Phys. Lett. B **105**, 125 (1981).

[42] F. G. Kondev, Nucl. Data Sheets **108**, 365 (2007).

[43] B. Singh, Nucl. Data Sheets **108**, 79 (2007).

[44] Zs. Podolyák *et al.*, CERN-INTC-2006-021, INTC-P-212, unpublished (2006).

[45] M. Bowry, ISOLDE newsletter, Spring (2011).

[46] S. W. Yates *et al.*, Phys. Rev. C **37**, 1889 (1988).

[47] Huang Xiaolong, Nucl. Data Sheets **110**, 2533 (2009).

[48] J. J. Valiente-Dobón *et al.*, Phys. Rev. C **69**, 024316 (2004).

[49] P. H. Regan *et al.*, Laser Phys. Lett. **1**, 317 (2004).

[50] A. I. Levon, Y. V. Nosenko, V. A. Onischuk, A. A. Shevchuk, and A. E. Stuchbery, Nucl. Phys. A **764**, 24 (2006).

[51] Zs. Podolyák *et al.*, Prog. Theor. Phys. Suppl. **146**, 467 (2002).

[52] V. R. Vanin *et al.*, Nucl. Data Sheets **108**, 2393 (2007).

[53] E. Achterberg, O. A. Capurro, G. V. Marti, V. R. Vanin, and R. M. Castro, Nucl. Data Sheets **107**, 1 (2006).

[54] X. Huang and C. Zhou, Nucl. Data Sheets **104**, 283 (2005).

[55] T. F. Thorsteinsen, J. S. Vaagen, G. Lovhoiden, N. Blasi, M. N. Harakeh, and S. Y. Van Der Werf, Nucl. Phys. A **435**, 125 (1985).

[56] Huang Xiaolong, Nucl. Data Sheets **108**, 1093 (2007).

[57] C. Zhou, Nucl. Data Sheets **86**, 645 (1999).

[58] Zs. Podolyák *et al.*, Phys. Rev. C **79**, 031305(R) (2009).

[59] L. M. Robledo, R. Rodríguez-Guzmán, and P. Sarriguren, J. Phys. G: Nucl. Part. Phys. **36**, 115104 (2009).

[60] N. Alkhomashi *et al.*, Phys. Rev. C **80**, 064308 (2009).

[61] M. S. Basunia, Nucl. Data Sheets **110**, 999 (2009).

[62] Zs. Podolyák *et al.*, Phys. Lett. B **491**, 225 (2000).

[63] G. F. Farrelly *et al.*, Acta Phys. Pol. B **40**, 885 (2009).

[64] G. J. Lane *et al.*, Phys. Rev. C **82**, 051304(R) (2010).

[65] M. W. Reed *et al.*, Phys. Rev. Lett. **105**, 172501 (2010).

[66] R. D'Alarcao *et al.*, Phys. Rev. C **59**, R1227 (1999).

[67] S. Zhu and F. G. Kondev, Nucl. Data Sheets **109**, 699 (2008).

[68] F. G. Kondev and S. Lalkovski, Nucl. Data Sheets **108**, 1471 (2007).